Spatiotemporal snow pattern in the Qilian Mountains from 2001 to 2018

Qiaodan Liu

TU Delft Delft University of Technology

Challenge the future

Front cover: A scene of the Qilian Mountains, Qinghai Province, China.

Spatiotemporal snow pattern in the Qilian Mountains from 2001 to 2018

by

Q. (Qiaodan) Liu

in partial fulfillment of the requirements for the degree of

Master of Science

in Civil Engineering

at the Delft University of Technology,

to be defended publicly on January 27, 2020.

Thesis committee:

Dr. Markus Hrachowitz (Chair), TU Delft

Dr. Thom Bogaard, TU Delft

Dr. Lisa Scholten, TU Delft

TU Delft Delft University of Technology

Content

Summary 1

1 **Introduction** 3

2 **Data overview** 7

2.1 Study area 7

2.2 Data sources 9

2.2.1 Remote sensing datasets 9

2.2.2 Digital elevation model (DEM) 11

2.3 The Google Earth Engine (GEE) 13

3 **Methodology** 14

3.1 The regional snow line elevation (RSLE) 14

3.2 Annual number of snow cover days (D_{sc}) 20

3.3 Sensitivity of D_{sc} to climatic and topographic factor 21

3.3.1 The climatic factor 21

3.3.2 The topographic factor 25

3.3.3 Temporal evolution of D_{sc} 26

4 **Results** 27

4.1 Regional snow line elevation (RSLE) 27

4.2 Spatial distribution of annual number of snow cover days 30

4.3 Temporal evolution of D_{sc} and the climatic factors 35

4.3.1 Evolution of annual snow cover days 35

4.3.2 The climatic factors 36

4.3.3 Relating D_{sc} to temperature and precipitation 37

4.4 Relating D_{sc} to hillshade 40

5 **Discussion** 42

5.1 Regional snow line elevation 42

5.2 Temporal evolution of D_{sc} 45

5.3 Relating D_{sc} to temperature and precipitation 46

5.4 Relating D_{sc} to hillshade 48

5.5 Review of the method 48

5.6 Further applications 49

6 **Conclusions** 50

Bibliography 52

A Sensitivities of annual accumulated precipitation 60

B Seasonality of D_{sc} and hillshade 62

Summary

In many parts of the world, water retained in snowpack and glaciers are critical to the stability of downstream ecosystems and human society. This study sets out to quantify, map, and explain the spatiotemporal pattern of annual snow cover duration, which are quantified by regional differences in the number of annual snow cover days (D_{sc}) and its sensitivities to climate change across the Qilian Mountains between 2001 and 2018. Here, D_{sc} is estimated using the MODIS snow product, based on the further development of the regional snow line elevation (RSLE) method, which is a filtering technique used to reduce the effects of cloud cover on a large scale.

The Qilian Mountains, based on the previous studies on regional climate difference, can be divided into three subregions from east to west. Across the entire Qilian Mountains, D_{sc} is about 20-40 days at elevations below 3500 m.a.s.l and increases to about 130 days at 4500 m.a.s.l, and more than 300 days above 5000 m.a.s.l. In the west, the interannual average D_{sc} is consistently lower than the east at the same elevation, and the largest difference is about 200 days at 4300 m.a.s.l. The middle subregion has its D_{sc} lower than the west below 4000 m.a.s.l, but higher above that elevation.

Throughout the 18 years, a 100-200 m upward shift of the RSLE in the hottest months (July and August) has happened in all the subregions of the Qilian Mountains, which certainly results in a decrease of snow cover area and duration. The statistical analysis indicates that on the 3500-4500 m.a.s.l hillside regions in the west section, the number of annual snow cover has the most pronounced decline of D_{sc} with a rate from -3 to -5 d/year, and this declining trend is caused by the 0.1-0.2 ℃/year increasing trend of the local land surface temperature.

The sensitivities analysis of D_{sc} to temperature and precipitation suggests that, in all the subregions, the annual mean temperatures T has a consistent first-order control on D_{sc} across the years. However, throughout the elevation, neither the temperature nor cold half-year precipitation has consistent first-order control on D_{sc}. On the contrary, the data highlight the importance of the interaction between the two climatic variables at 3500-5000 m.a.s.l, where D_{sc} is sensitive to local climate change. In this elevation range, the positive effects of cold half-year precipitation increasing may partly compensate for the negative effects of temperature rising on D_{sc}. Furthermore, since the lack of precipitation

in the west section, the interplay between temperature and precipitation has its influence on D_{sc} mostly in the east section, and as a consequence, the significant reduction of D_{sc} in a large area only happens in the west of the Qilian Mountains.

Moreover, we look into the correlation between D_{sc} and the hillshade and get an interesting result that the medium-hillshade regions, but not the lightest regions, always have the lowest D_{sc}. The possible reason for this phenomenon is that the lightest regions are more likely the peaks of the mountains i.e. glaciers, while the medium-hillshade regions are more likely the hillshade at low or medium elevation.

1 Introduction

In many parts of the world, the accumulation of water in seasonal snow is critical to maintaining downstream ecosystems, including human society, especially in the northern hemisphere (Mankin et al., 2015). Snow melting not only affects the timing and scale of spring floods (Parajka et al., 2010), but also maintains summer flow in many regions (Mankin et al., 2015), and is, therefore, an important part of water management e.g. for human consumption, industrial and agricultural production, hydro-power production (Madani and Lund, 2010). Besides, and perhaps most importantly, snow is a key component of regional and global energy budgets because its high reflectivity reflects most of the incident short-wave solar radiation, providing an effective buffer for global warming (Déry and Brown, 2007; Fernandes et al., 2009).

However, global warming gradually affected the hydrological cycle through the increase of water vapor in the lower troposphere (Held and Soden, 2006), which severely affected seasonal snowfall. This will have a significant impact on the allocation between evaporative flux and drainage (Berghuijs et al., 2014; Gao et al., 2014), and may put a significant portion of the water available in seasonal snow at risk (Mankin et al., 2015). Leading to changes in hydrological conditions (e.g. Barnett et al., 2005; Hrachowitz et al., 2013; Berghuijs et al., 2014), and changes in the characteristics of extreme events (Laaha et al., 2016).

Snow cover and snowmelt dynamics are characterized by a large amount of spatiotemporal heterogeneity within a certain range (Déry et al., 2004). In addition to the general dependence of snow on temperature, they are also controlled by a variety of interaction factors, including precipitation (Hrachowitz and Weiler, 2011), wind-induced snowdrifts (Dadic et al., 2010), and solar radiation (Rinehart et al., 2008), terrain (Jost et al., 2007), vegetation (Ellis et al., 2010), artificial snow accumulation (Steiger, 2010). In regional or larger studies, snow is typically characterized using more easily observed, lower-dimensional measures, e.g. snow depth (e.g. Deems et al., 2013; Kunkel et al., 2016), and snow duration (e.g. Hantel and Hirtl-Wielke, 2007; Allchin and Déry, 2017; Hori et al., 2017) or snow-cover areas (e.g. Brown and Robinson, 2011; Mudryk et al., 2017). Most of the results of these studies also show that in the past decades, various snowfall indicators have been highly sensitive to climate change and related negative but

local trends. To date, many studies have relied on estimates obtained from model applications or direct ground observations and related limitations to quantify these snow measurements, including model uncertainty and limited spatial resolution of observations (e.g. Zeng et al., 1987; Guo et al., 2003). However, with the latest developments in technology, more and more studies of the potential of snow mapping using remote sensing products have been conducted in this century (e.g. Han et al., 2011; Jiang et al., 2016).

Although there are typical limitations related to remote sensing, e.g. cloud cover (Parajka and Blöschl, 2006), they have been proven to be valuable data sources for snow climate applications due to their potential to provide information on snow cover in space and time (Immerzeel et al., 2009). For example, weekly data from ultrahigh-resolution high-resolution radiometer (AVHRR) data from the National Oceanic and Atmospheric Administration (NOAA) in the past have been used in continental-scale analysis to determine the number of snow cover days (D_{sc}) per year is used as a global snow-related variable and is most sensitive to change (Brown and Mote, 2009). However, the product has a relatively coarse spatial resolution (for the latest images, the highest resolution is 1 km) cannot be analyzed in greater detail, especially in mountainous areas. The time resolutions from the Sentinel 2 and LANDSAT missions of 2-3 and 16 days, respectively, do not provide sufficient time resolution to capture snow and Snow dynamics during depletion, but they have a high spatial resolution (e.g. 30 meters) that have previously proven valuable for testing other snow products (Crawford et al., 2015; Rittger et al., 2013). In contrast, Moderate Resolution Imaging Spectroradiometer (MODIS) snow products (i.e. Terra MOD10A1; Hall et al., 2002) have the next-day temporal resolution and 500 m spatial resolution, which is a compromise solution that can provide enough detail for both to understand the patterns of spatial snow cover and its temporal dynamics. Since their first release in September 2000, they have often been used for various types of climatological or hydrological studies (e.g. Andreadis and Lettenmaier, 2006; Dietz et al., 2012; Tomaszewska and Henebry, 2018).

Assessments against ground station data in different regions found overall accuracy-levels for non-cloud-filtered imagery ranging from 93% (Hall and Riggs, 2007) to 95% (Parajka and Blöschl, 2006), with lowest values at forested sites (Parajka et al., 2012). A range of methods to deal with cloud-obscuration has been developed and tested, mostly

keeping high accuracy levels, including the combination of Terra and Aqua snow cover products, spatiotemporal filtering, use of snow depth data and snow-line filtering (Dietz et al., 2012; Dong and Menzel, 2016; Gafurov and Bárdossy, 2009; Parajka and Blöschl, 2008). A very efficient cloud filter, with an overall accuracy of 86%, was introduced with the Regional Snow Line Elevation (RSLE) method by Krajci et al. (2014). The RSLE method is a spatial filter that largely preserves temporal information and potentially produces spatially consistent, “gap-free” time-series of snow line elevation, that can be used directly for various further applications. In doing so, Krajčí et al. (2016) analyzed snow line dynamics, snow-covered area, and snow depletion curves for 10 catchments in Slovakia for the period 2001 to 2014.

To understand the impact of climate change on seasonal snow, seasonal snow may have great spatial heterogeneity on the continent (e.g. Mankin et al., 2015), but on a regional scale (e.g. Huning and AghaKouchak, 2018) It is essential to make a strong quantitative regional description of the sensitivity of snow cover to climate change, especially temperature and precipitation and their interactions.

Various studies have been done on the variability in the snow cover in the Qilian Mountains. Zeng et al. (1987) analyzed the AVHRR data in 1980-1985 and found 3700 meters above the sea level (m.a.s.l.) as the snow line elevation in winter and spring. Chen et al. (1991) studied data from 28 meteorological observing stations and AVHRR from 1951 to 1988 and obtained the mean annual amount of snow was 160.5×10^8 m^3, whereas the mean spring (April to May) snow water storage and snowmelt runoff (late-March to early-June) were estimated to respectively account for 10.9% and 7.8% of the mean annual snowfall. Wei et al. (2002) analyzed the data of snow depth from 72 weather stations in Qinghai Province and found that in the Qinghai Lake Basin the snow started in October or November and ended in May or June. Guo et al. (2003) found the snow area decreased 2.17% in the west of the Qilian Mountains and 10.05% in the east of the mountains from 1989 to 1998, and the ten-day averaged snow area was decreased in the whole area. Zhang et al. (2005) revealed that the snow-cover area and the snow line elevation changed obviously with global and regional climate change, especially in the middle section of the Qilian Mountains. Cai et al. (2009) studied MODIS data in the Qilian Mountains from 1960 to 2005 and found the snow cover supply in the area over 4000 m.a.s.l appeared mainly in spring and fall, and the duration increased with elevation,

while in lower elevation the snow appeared only from middle fall to middle winter. Wang et al. (2010) noticed that the snow cover frequency in the western and the eastern subregion of the Qilian Mountains increased with the elevation, while the situation in the middle subregion was more complicated. Han et al. (2011) found that the eastern and the middle snow area in the Qilian Mountains showed a declining trend from 1997 to 2006 and the eastern snow of the Qilian Mountains was mostly influenced by local climatic conditions. Jiang et al. (2016) indicated that snow cover in the western region was significantly greater than that in the east, and the snow cover was more sensitive to precipitation in the winter, while temperature and precipitation were the major factors that affected the snow cover in the spring.

The conclusions of the previous studies in the Qilian Mountains indicate that the characteristics of the snow cover in the east, middle and west subregions of the Qilian Mountains are different. However, most of the past studies have relied on either relatively coarse-resolution model output or relatively sparse ground station observations, so at least the local and local spatial heterogeneity in the snow accumulation process may be lost. To reduce the gap between the observation range and resolution, which is necessary to improve and seamlessly understand the spatial heterogeneity of snow dynamics at the regional scale, we will further develop the RSLE method in this study as a large scale method. Using MODIS snow data covering the entire Qilian Mountains area, the large-scale cloud reduction method was used to estimate the snow duration. The overall goal of this study is to provide, for the first time, a detailed, near-seamless, high-resolution, and data-only analysis of regional differences in annual snow durations D_{sc} and their sensitivity to interannual changes in temperature. And precipitation exceeds the catchment scale. More specifically, the purpose of this study was to discover:

(1) whether there are any systematic regional differences in the annual number of days with snow cover duration (D_{sc}) across the Qilian Mountains;

(2) whether the climatic characteristics i.e. temperature and precipitation, and topography properties i.e. hillshade have any effects on the snow cover duration i.e. D_{sc} in different subregions;

(3) whether the regional differences in D_{sc} temporal trends over the 2001-2018 study period can be explained by the different regional climatic properties.

2 Data overview

2.1 Study area

The Qilian Mountains are located in the northeastern margin of the Tibetan Plateau, extending from Wushaoling westward to Dangjin Shankou, connected to the Altun Mountains, and are composed of a series of the northwest to southeast mountains and valleys on the border of Gansu Province and Qinghai Province. The range stretches from the south of Dunhuang some 800 km to the southeast, forming the northeastern escarpment of the Qinghai-Tibetan Plateau. (You et al., 2013) The highest peaks of the seven parallel mountain lines are equally distributed between 5153 and 5827 m.a.s.l. The eponymous Qilian Mountain Peaks is located about 60 kilometers south of Jiuquan, and the east longitude is 39°12′N 98°32′E, rising to 5547 m.a.s.l. It is the highest peaks of the main range, but there are To higher peaks in the south, the Corniche is at 38°30′N 97°43′E, 5808 m.a.s.l, and the Qaidam Peaks is at 38°2′N 95°19'E and 5,759 m.a.s.l. Other major peaks include the Gangshicha Peaks in the east. The Nanshan Mountains continue to extend westward, namely Yema Mountain (5250 m.a.s.l) and Altyn Tagh (5798 m.a.s.l). To the east, it passes north of the Qinghai Lake and ends in Dazhou and Xinglong Mountain near Lanzhou. The eastern mountain is the peaks of Maoma Mountain (4070 m.a.s.l). (Wang et al., 1981)

the Qilian Mountains are uninhabited from the root of the mountains, with only several counties located in the mountain valleys in the eastern end. The northernmost foothills are dozens of kilometers away from the Hexi Corridor, and southernmost mountains are the northern outlier of the Kunlun Mountains. The rest of the mountainous areas are the no man's land. the Qilian Mountains are the source of numerous, mostly small, rivers and creeks that flow northeast, enabling irrigated agriculture in the Hexi Corridor communities, and eventually disappearing in the Alashan Desert. The best known of these streams is the Heihe River. The region has many glaciers, the largest of which is the Touming Mengke (Wang et al., 1981). The region lies in a transitional zone between arid northwestern China and the Qinghai-Tibetan Plateau. Thus it is controlled by westerly winds in the west where precipitation is sparse and affected by the Asian summer monsoons in the east where precipitation is relatively abundant. Precipitation is mainly concentrated in the warm half-year, and the annual precipitation and warm-season

precipitation all show trends of decreasing from east to west. The drainage system in the mountains is oriented from northwest to southeast. (Tian et al., 2017; Sun et al., 2018)

In some research on the precipitation in the Qilian Mountains(Tang et al., 1985; Zhang et al., 2004; Jia et al., 2008), the Qilian Mountains region can be divided into three subregions the red straight line in figure 1. However, the particular position of the boundary is not clear in the previous studies. Instead, the location of the weather stations is used as a reference of the boundary (red stars in the figure). From west to east, the location of the three stations are: Tuole station, boundary between the west and middle subregions, 38°48’ N 98°25’ E; Qilian station, boundary between the middle and east subregions, 38°27’ N 100°49’ E; Menyuan station, boundary between the middle and east subregions, 37°23’ N 101°37’ E. Based on the location of the three stations, the Qilian Mountains is divided into three subregions: west section, from 94° to 98° E; middle section, from 98° to 101° E; east section, from 101° to 103° E. Figure 1 shows the subregion separation of the study area.

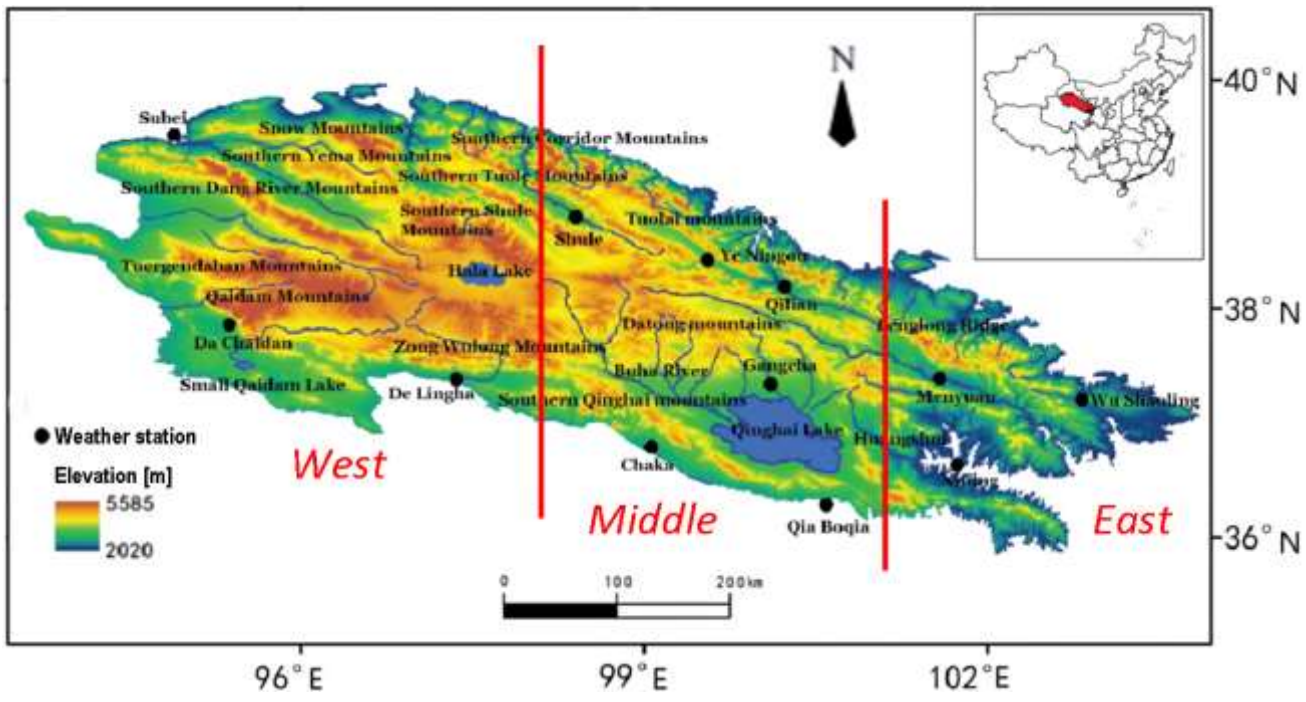

Figure 1. Spatial distribution of meteorological stations in the Qilian Mountains

With the increase of precipitation by 10%–20% per decade in northwestern China since 1950 (Zhai et al., 2005), the variability of snow cover in this area has become a hot issue in response to climate change, including the spring flood, regulation of water resources, and living and production of the people. Qinghai Lake, the largest saline lake with an

area of 4,260 km^2 (2000) and an average depth of 21 meters (1985) in west China, is surrounded by the Qilian Mountains in Qinghai Province. It is located in the joint area of the East Asian monsoon, Indian summer monsoon, and Westerly jet stream, and particularly sensitive to climate change (Shi et al., 2007). Li et al. (2007) found that water consumption by human activities accounted for 1% of the evaporation loss of the lake and had an ignorable influence on the lake's water balance. The surface area of the lake shrank from 1974 to 2004 but expanded sharply after that (Luo et al., 2017). Zhang et al. (2011) indicated that the longest period of lake level increase was from 2004 to 2009 and it might be due to accelerated glacier/perennial snow cover melting in the Qilian Mountains area during recent decades.

2.2 Data sources

2.2.1 Remote sensing datasets

Sources of remote sensing datasets

The MODIS/Terra Snow cover Daily Global 500 m (MOD10A1 V6) is from the U.S. National Snow and Ice Data Center (https://nsidc.org/). It contains snow cover, classification of the snow cover, snow albedo, fractional snow cover, and quality assessment (QA) data. Snow cover data are based on a snow mapping algorithm that employs a Normalized Difference Snow Index (NDSI) and other criteria tests.

The MODIS/Terra MOD11A2 V6 product provides an average 8-day land surface temperature (LST) in 1 km spatial resolution. Each pixel value in MOD11A2 is a simple average of all the corresponding MOD11A1 daily LST pixels collected within those 8 days. The LST dataset is from NASA's Land Processes Distributed Active Archive Center (https://lpdaac.usgs.gov/). The 8-day compositing period was chosen because Tice that period is the exact ground track repeat period of the Terra and Aqua platforms. In this product, along with both the day- and night-time surface temperature bands and their quality indicator (QC) layers, are also MODIS bands 31 and 32 and eight observation layers.

Global Precipitation Measurement (GPM) from NASA (https://www.nasa.gov/) is an international satellite mission to provide next-generation observations of rain and snow

worldwide every three hours. The integrated multi-satellite retrievals for GPM is the unified algorithm that provides rainfall estimates combining data from all passive-microwave instruments in the GPM constellation. This algorithm is intended to intercalibrate, merge, and interpolate all satellite microwave precipitation estimates, together with microwave-calibrated infrared (IR) satellite estimates, precipitation gauge analyses, and potentially other precipitation estimators at the fine time and space scales for the Tropical Rainfall Measuring Mission (TRMM) and GPM over the entire globe. The system is run several times for each observation time, first giving a quick estimate and successively providing better estimates as more data arrive. The final step uses monthly gauge data to create research-level products.

Validation of remote sensing datasets

The meteorological stations in the Qilian Mountains do not keep snow cover observation but do have a record of temperature and precipitation. Based on these measures, some studies about the comparison of remote-sensing data with local station observed data in the Qilian Mountains has been done for the MODIS land surface temperature and TRMM/GPM precipitation in recent years. The following studies show that remote sensing climate data has some bias but significant correlations and similar trends compared to the station observed data.

Ke et al. (2011) compared the LST with the maximum air temperature observation at 62 meteorological station in 2008 in Northeast Qinghai-Tibet Plateau (QTP) which contains the Qilian Mountains as half of the study region and indicated that the LST is significantly correlated with maximum air temperature with a correlation coefficient of 0.88. LST has a 6.98 °C (in root-mean-square deviation, RMSD) bias over maximum air temperature on average. In general, for every 1000 meters increasing in elevation, the deviation between LST and maximum air temperature increases by 1 °C. Yu et al. (2011) compared the LST with the observed maximum air temperature of several stations with different land cover types in the Qilian Mountains in 2008 and suggested that the MODIS data suits the observation better at night, and the mean absolute error is less than 2.2 °C in the studied stations.

Sun et al. (2019) compared the TRMM/GPM data with the observed precipitation data from 27 meteorological stations from 1998 to 2016 and found that the TRMM data has

strong correlations of the observed precipitation with an average adjusted R-square around 0.8. The linear regression on the annual accumulated precipitation with an adjusted R-square of 0.94 shows that the observed precipitation is mostly higher than the TRMM data when the observation is lower than 300 mm/year and vice versa. The linear regression on the seasonal accumulated precipitation indicates the value of R-square of 0.89, 0.88, 0.87 and 0.70 for summer, autumn, spring, and winter, respectively. The seasonal analysis shows that TRMM performs well in summer but underestimates the accumulated precipitation in other seasons on different levels.

2.2.2 Digital elevation model (DEM)

The Global Multi-resolution Terrain Elevation Data 2010 (GMTED2010) dataset from the U.S. Geological Survey (https://www.usgs.gov/) contains global elevation data collected from various sources. The version of the DEM dataset used in this research is breakline emphasis, 7.5 arc-seconds resolution. Breakline emphasis maintains the critical topographic features e.g. streams and ridges within the landscape by maintaining any minimum elevation or maximum elevation value on a breakline that passes within the specified analysis window.

The primary source dataset for GMTED2010 is NGA's SRTM Digital Terrain Elevation Data (DTED, http://www2.jpl.nasa.gov/srtm/) 1-arc-second data. For the areas outside the SRTM coverage area and filling the voids in the SRTM data, the following sources are used: non-SRTM DTED, Canadian Digital Elevation Data, Satellite Pour l'Observation de la Terre Reference 3D, National Elevation Dataset for the continental United States and Alaska, GEODATA 9 second digital elevation model for Australia, and Antarctica satellite radar and laser altimeter DEM, and a Greenland satellite radar altimeter DEM.

Figure 2 shows that the highest mountain peaks, where the glaciers appear, are mostly located in the west and east section. The west section has a much higher average elevation than the other two sections, and the north area is higher than the south. Moreover, in the north part of the Qilian Mountains, a belt-like area shows a high elevation difference.

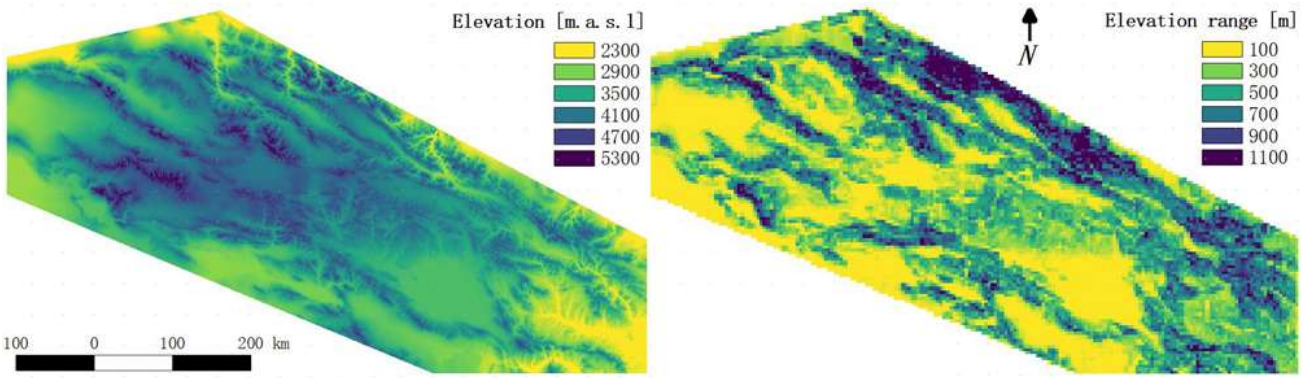

Figure 2. The elevation (left) and elevation range in 5 x 5 km² tiles (right)

Figure 3 indicates that the areas lower than 2500 m.a.s.l or higher than 5000 m.a.s.l are very small. For regions below 2500 m.a.s.l, the MODIS observation error is considerable due to the small total area, even a small observation change will lead to great fluctuation in the result, especially in the warm half-year in the middle section. The regions above 5000 m.a.s.l are free from this problem because they are always likely to be glaciers. For the above reason, the elevation range used in this study will be 2500-5500 m.a.s.l. Table 1 shows an overview of all the data sources used in this study.

Snow	MODIS Global Daily Snow cover (MOD10A1) https://nsidc.org/data/MOD10A1
Land Surface Temperature	MODIS average 8-day Land Surface Temperature (MOD11A2) https://lpdaac.usgs.gov/products/mod11a2v006/
Precipitation	Global Precipitation Measurement (GPM), including the Tropical Rainfall Measuring Mission (TRMM) https://pmm.nasa.gov/gpm
Terrain	The Global Multi-resolution Terrain Elevation Data 2010 (GMTED2010) https://www.usgs.gov/centers/eros/science/usgs-eros-archive-digital-elevation-global-multi-resolution-terrain-elevation?qt-science_center_objects=0#qt-science_center_objects

Table 1. The data sources

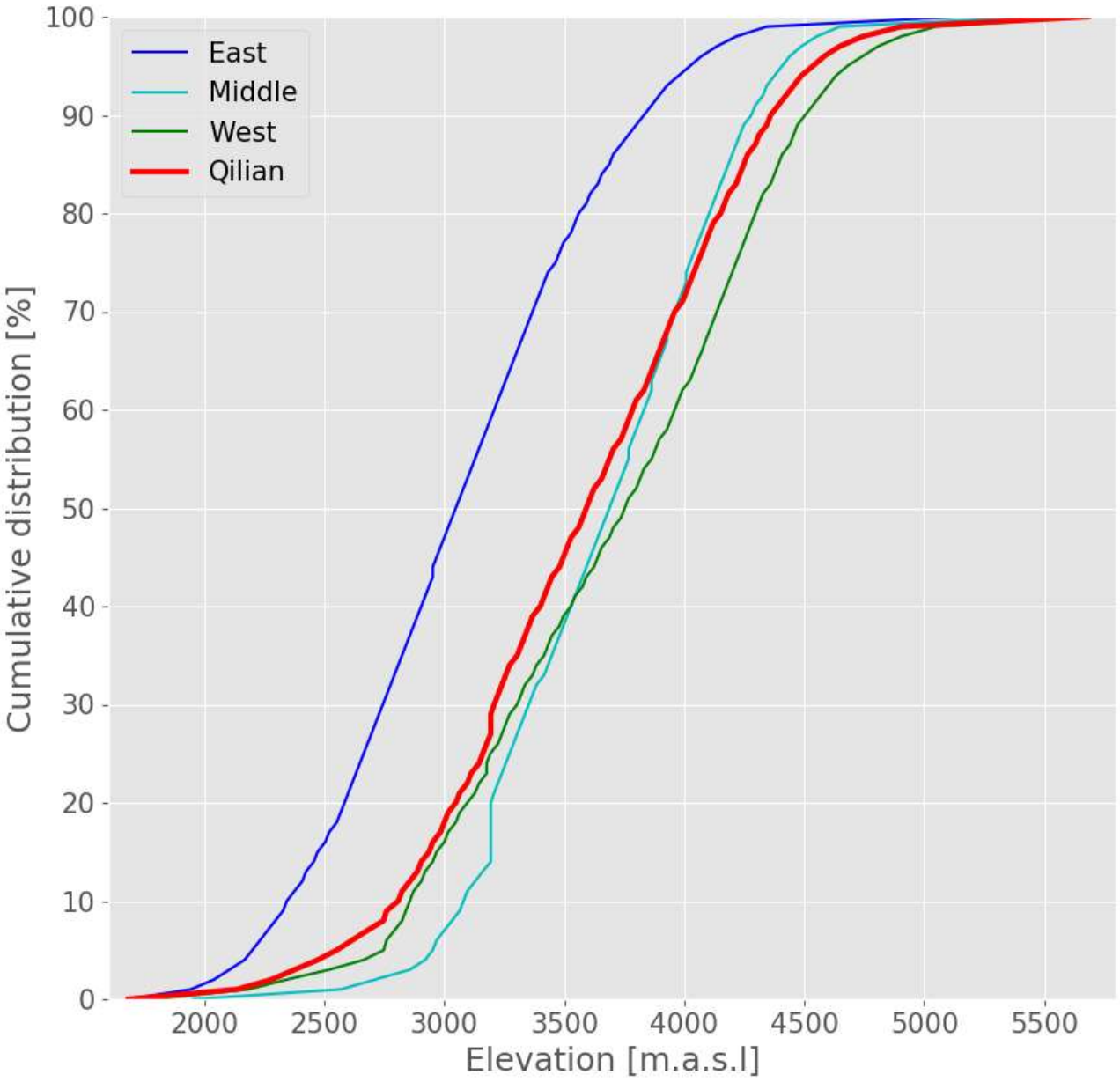

Figure 3. Hypsometric curves of the Qilian Mountains

2.3 The Google Earth Engine (GEE)

GEE is a cloud-based platform for scientific planetary-scale environmental data analysis and visualization of geospatial datasets, for academic, non-profit, business and government users. The purpose of the Earth Engine is performing highly-interactive algorithm development at a global scale, pushing the edge of the envelope for big data in remote sensing, enabling high-impact and data-driven science, and making substantive progress on global challenges that involve large geospatial datasets. Earth Engine hosts satellite imagery and stores it in a public data archive that includes historical earth images.

The images, ingested daily, are then made available for global-scale data mining. GEE has a searchable data catalog, including the entire Earth Resources Observation and Science (USGS/NASA) Landsat catalog, numerous MODIS datasets, Sentinel-1 data, precipitation data, sea surface temperature data, and elevation data.

GEE is built on JavaScript instead of Python or Fortran which are commonly used in hydrology analysis. Comparing to the common platforms, on the one hand, GEE has obvious advantages in some area: It can easily import a large amount of remote sensing data e.g. daily data through decades and that means no need to collect and download data from different websites which always spends some time and storage on the local computer; Earth Engine can use the servers in Google clusters to do the computation which is always faster than the individual computer in local; the result of the computation is directly exported to the cloud like Google Drive and automatically backed up; JavaScript is convenient to deal with the remote sensing data as images because of its property. On the other hand, GEE has some weakness: The JavaScript does not perform a very high precision in numerical computation, which is a major problem when the grid is built manually but not automatically; the Google clusters are sometimes attacked and not working for several days; the collection of datasets loses some datasets e.g. MODIS/Terra Snow cover 8-Day Global 500 m (MOD10A2 V6); moreover, GEE is different from Python or Fortran and learning it costs some time, perhaps weeks or months.

3 Methodology

3.1 The regional snow line elevation (RSLE)

Parajka et al. (2010) introduced the RSLE method to generate time-series of the average snow line elevation from partially cloud-obscured remote sensing images and it was used for estimating snow cover in cloud-covered basins (Krajčí et al., 2014 and 2016). The cornerstone of the method is to find an elevation (RSLE) for which the sum of snow-cover pixels below (P_s) and land pixels above the RSLE (P_l) is minimized. For each time step t (always in days), The algorithm loops the elevation $h_i$from the minimum elevation h_{min} to the maximum elevation h_{max} of all pixels in a specified domain with a chosen elevation step e.g. 1 meter and minimizes the objective function

$$F(h_i) = P_s(h_i) + P_l(h_i) \quad (1)$$

For every region in the study domain at day t, the elevation with the minimum $F(t)$ is then defined as the regional snow line elevation (RSLE) for the day. The analytical conditions for $F(h_i)$ to be minimum are given by annulling the first derivative in the objective function (steady-state condition) and imposing a positive second derivative in the objective function (positive inflection) at the steady states. Mathematically, these conditions can be written as:

$$\frac{\partial F(h_i)}{\partial h_i} = \frac{\partial P_s(h_i)}{\partial h_i} + \frac{\partial P_l(h_i)}{\partial h_i} = 0 \quad (2)$$

$$\frac{\partial^2 F(h_i)}{\partial {h_i}^2} = \frac{\partial^2 P_s(h_i)}{\partial {h_i}^2} + \frac{\partial^2 P_l(h_i)}{\partial {h_i}^2} > 0 \quad (3)$$

In the previous studies, these equations were solved numerically with finite elevation differences of a 1-meter interval between h_{min} and h_{max}. However, considering GEE is well in statistical analysis but poor in numerical looping for images, using elevation cumulative distribution function (CDF) is easier and faster than directly using the numerical elevation. That means the RSLE is not estimated directly as an elevation, but firstly estimated as the percentiles in the elevation CDF and then acquired as the numerical elevation as shown in figure 2. The 1-meter interval of finite elevation differences is now replaced by a 1% interval in the elevation CDF.

In this study, since the Qilian Mountains domain (36° - 40° N and 94° - 103° E) is much larger than a common river basin in the previous studies, the RSLE method cannot be applied directly but in several steps, as shown in figure 4. Firstly, the study domain must be split into smaller spatial sub-domains referred to as ‘tiles’ to apply the RSLE method. The most suitable size of the tiles, worded differently the number of individual MODIS pixels to be aggregated to obtain a meaningful estimation of individual RSLE in each tile, has to be identified. The tile size is the key to the RSLE method using elevation CDF because with the fixed 1% interval in elevation CDF, a larger elevation range means a larger elevation interval corresponding in numerical and undoubtedly leads to a coarser result. On the one hand, small tiles lead to a high spatial resolution and elevation precision in the result but increase the amount and length of the data-loss gaps brought by cloud obstruction in the RSLE time-series. On the other hand, the larger the tile, the

more natural variability of snow line elevations within the tile would be averaged out and concealed by the RSLE method, causing a loss in spatial resolution and elevation precision, but the negative influence from cloud obstruction is reduced. As an illustration, in a hypothetical ideal case of completely cloud-free observations, no aggregation will be needed, and the number of snow cover days (D_{sc}) can be directly calculated. In this case, the RSLE time-series is replaced by continuous gap-free binary time-series of snow cover or non-snow cover, and the tile size will reduce to the 500-m pixel scale of the MODIS observation.

Different tile sizes (5 x 5 km^2, 10 x 10 km^2, 15 x 15 km^2, and 20 x 20 km^2) are applied to see which one is the best choice of the tile size. For every tile size, the discontinuous RSLE time-series and the map of D_{sc} are obtained for the year 2015. For the RSLE time-series from different tile sizes, statistical analysis for the length and number of the gaps i.e. missing values, and for the D_{sc} map the differences in each pixel among the tile sizes are obtained by subtraction or division. From this analysis, the large tiles do not significantly reduce the number and length in the RSLE time-series since the cloud in the Qilian Mountains usually covers a large area and is spatially continuous. In other words, the cloud tends to cover many neighbor tiles even the tiles are large. However, the large tiles do conceal some details of the spatial D_{sc} variation, especially at the margin of the glaciers. As a balanced compromise between spatial details of the D_{sc} and the control of missing values in the RSLE time-series, a tile size of 10 x 10 pixels (5 x 5 km^2) is chosen for this study, and it is the smallest tile size acceptable when using elevation CDF method because 100 pixels in a tile is likely perfectly corresponded by a CDF with 1% as the interval. For the local machine, computation time is critical for the choice of tile size, but it is less important for GEE. The smallest 5 x 5 km^2 tile has an average computation time of fewer than 3 hours for a one-year time period, which is acceptable for this study.

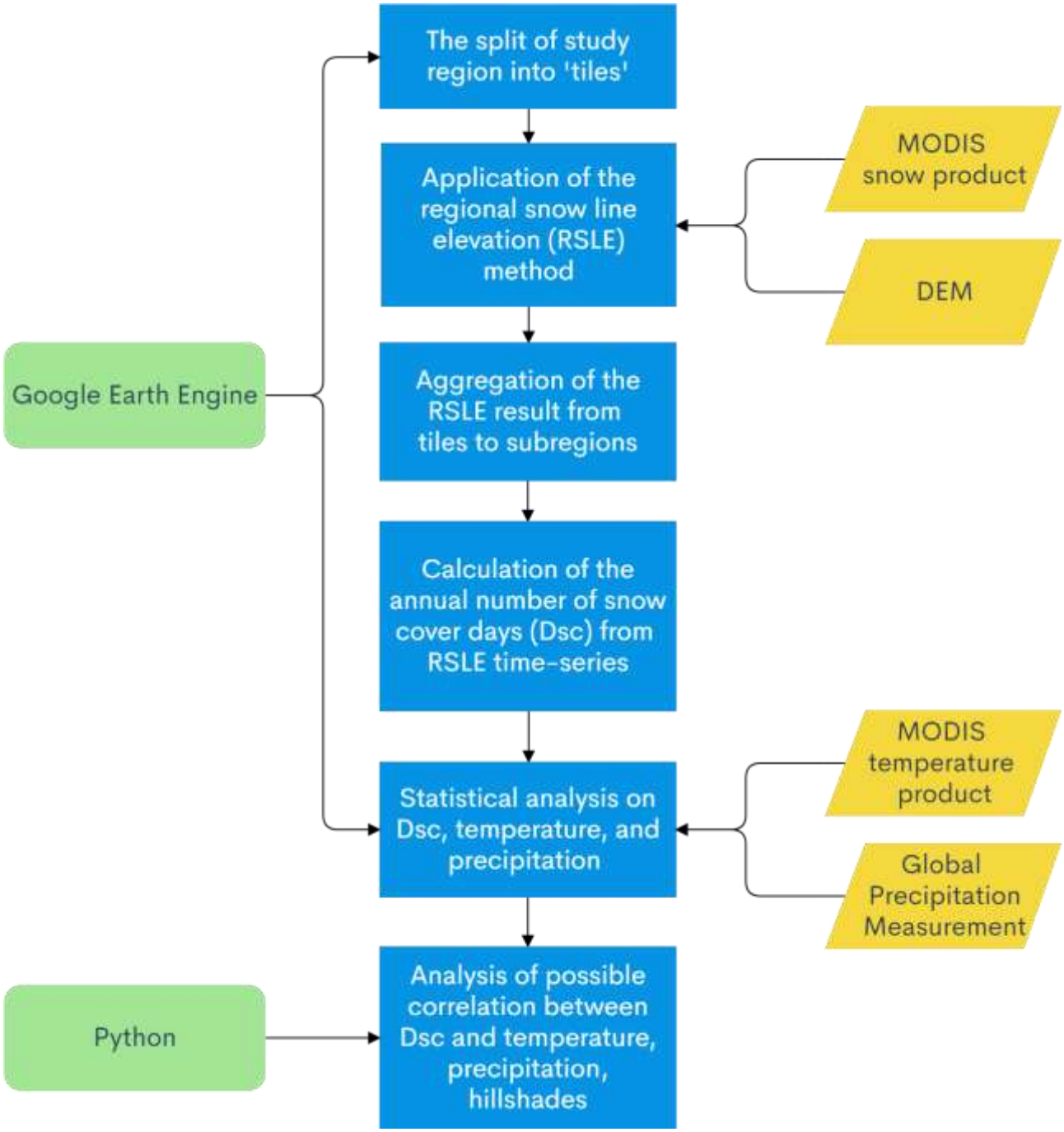

Figure 4. Flowchart of the analysis

The RSLE method is applied with the MODIS/Terra Snow cover Daily Global 500 m (MOD10A1, Version 6) images and the DEM image (GMTED2010). All the images are firstly reprojected into 500-m pixels and a coordinate system EPSG:3857 using the average value to make sure the geographic locations of the pixels correspond correctly. The DEM is then divided into 101 images with the minimum (0%) and maximum (100%) elevation in the elevation CDF for each tile. The MOD10A1 provides gridded values of normalized difference snow index NDSI values ranging from 0 to 100. Härer et al. (2017)

indicated a snow detection threshold of NDSI = 40 to discriminate between ‘snow’ and ‘no-snow’ in general but in real life, this threshold may change from one place to another. In this study, we use NDSI = 33 as the snow detection threshold for the Qilian Mountains suggested by Hao et al. (2008).

Figure 5 shows that MODIS does observe snow cover areas on the Qinghai Lake in summer and autumn i.e. on July 1st (the areas in red circles), but the surface temperature of the Qinghai Lake in warm half-year is always higher than 5 ℃, which means the ice cannot exist on the lake. The reason for this performance, as well as an essential parameter linking to the RSLE result, is the basic estimate of the quality in the MODIS snow product. In MOD10A1, the NDSI_Snow_Cover_Basic_QA is a basic estimate of the quality of the algorithm result which is computed for MOD10_L2 and retrieved with the corresponding observation of the day. The observation with ‘OK’ reports some snow cover on the Qinghai Lake in summer which is unreliable, while the ‘Good’ has less unreliable observation and can be eliminated in the later process. Thus, in this study only the observation with quality above ‘OK’ i.e. ’Good’ and ‘Best’ are used.

To ensure the robustness of the RSLE, after some tests the maximum cloud-cover threshold for a reliable observation is fixed at 70%. If the fraction of cloud covered pixels for a given tile at a specific time step is greater than 70% of the total number of pixels in the tile, the tile is flagged as ‘cloud-cover’ for this time step. The choice of maximum cloud-cover threshold is guided by the sensitivity analysis performed by Krajci et al., (2014). Similarly, a minimum snow cover threshold is fixed to limit small scale misclassification of snow. The study of Krajci suggested that the minimum snow cover threshold based on the ratio between the number of snow cover pixels and the total number of pixels in the tile would significantly limit the utility of the cloud coverage threshold. In the preliminary test of this study, it gives an incorrect result in the warm half-year e.g. RSLE reaches its lowest point. To solve this problem the minimum snow cover threshold is now based on the number of cloud-free pixels instead of the total number of pixels in the tile. That is, for the tiles with the same number of snow cover pixels, assuming the cloud cover is random, the more cloud-free pixels observed, the more snow-cover it should be.

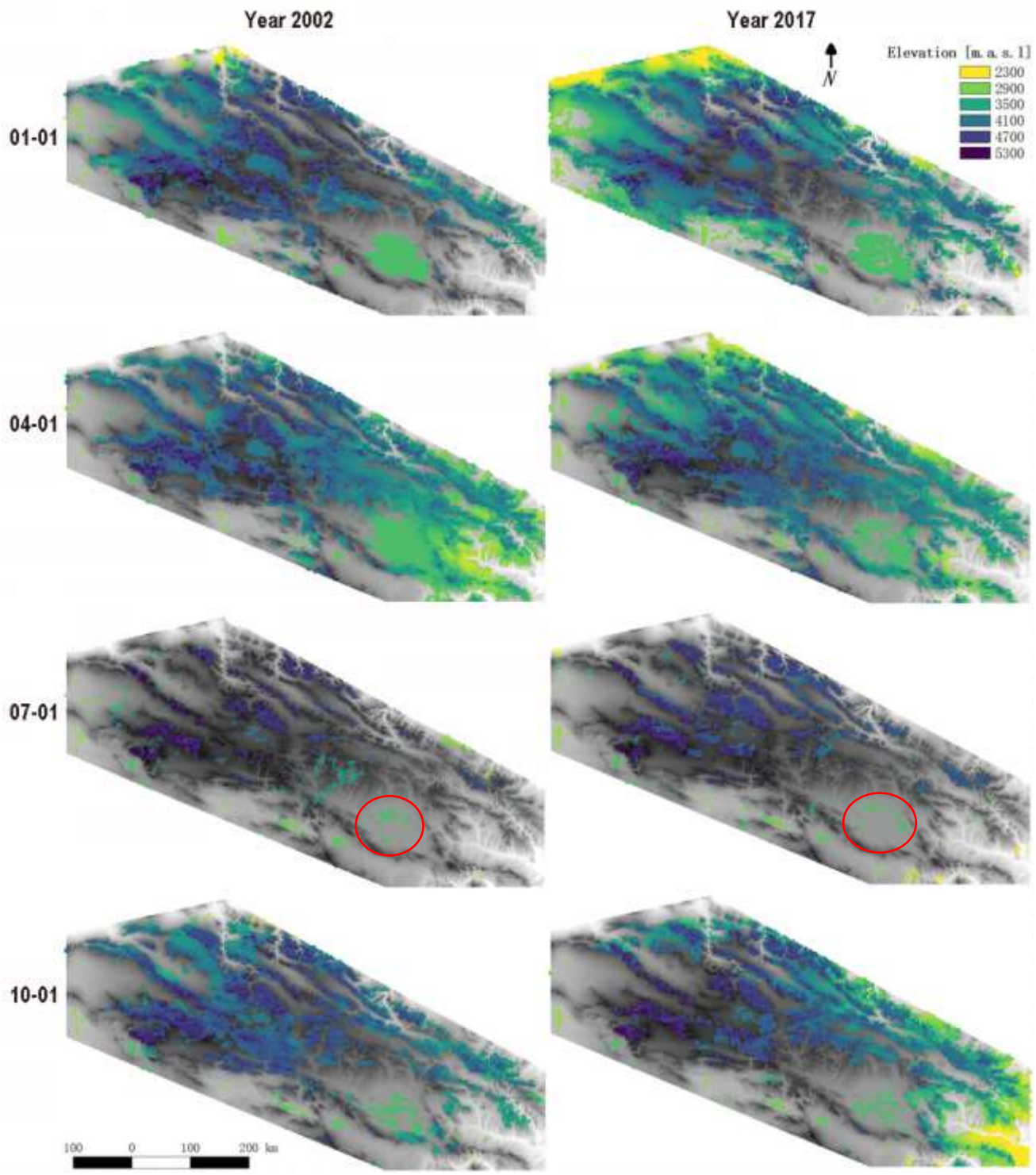

Figure 5. The non-gap-filling RSLE across the Qilian Mountains on January 1st, April 1st, July 1st, October 1st for the year 2002 and 2017 with the elevation map as the background

For each tile, the RSLE time-series is firstly gap-filled using linear interpolation to get a continuous time-series for the next steps. For a meaningful interpretation, the noise in the original daily RSLE time-series of each tile caused by accidental and cognitive errors (e.g. cloud cover) is smoothed according to the following filters:

$$\mathrm{RSLE(t)} = \begin{cases} \mathrm{RSLE(t)}, & |\mathrm{RSLE(t)} - \mathrm{RSLE(t-1)}| \text{ and } |\mathrm{RSLE(t)} - \mathrm{RSLE(t+1)}| \leq \Delta\mathrm{RSLE_{crit}} \\ 0, & |\mathrm{RSLE(t)} - \mathrm{RSLE(t-1)}| \text{ and } |\mathrm{RSLE(t)} - \mathrm{RSLE(t+1)}| > \Delta\mathrm{RSLE_{crit}} \end{cases} \quad (4)$$

where $\Delta\mathrm{RSLE_{crit}}$ is a maximum acceptable difference of RSLE at time step t to the respective values at one day before i.e. $\mathrm{t}-1$, and the next day $\mathrm{k}+1$. After some tests, considering about the tile size and the elevation range in the tiles, the $\Delta\mathrm{RSLE_{crit}}$ in this study is set to 100 meters to make sure the RSLE does not change more than 100 meters in one day. The familiar filters can be applied for varies period:

$$\mathrm{RSLE(t)} = \begin{cases} \mathrm{RSLE(t)}, & |\mathrm{RSLE(t)} - \mathrm{RSLE(t-n)}| \text{ and } |\mathrm{RSLE(t)} - \mathrm{RSLE(t+n)}| \leq \Delta\mathrm{RSLE_{crit}(n)} \\ 0, & |\mathrm{RSLE(t)} - \mathrm{RSLE(t-n)}| \text{ and } |\mathrm{RSLE(t)} - \mathrm{RSLE(t+n)}| > \Delta\mathrm{RSLE_{crit}(n)} \end{cases} \quad (5)$$

where n is the period under control. When $\mathrm{n} = 7$, the change of RSLE in one week cannot exceed $\Delta\mathrm{RSLE_{crit}}(7)$. Intuitively, the value of $\Delta\mathrm{RSLE_{crit}(n)}$ increases as the value of n increases. In this study, the maximum value of n is 5 days and the value of $\Delta\mathrm{RSLE_{crit}}(5)$ is set as 500, which means a 5-day 500-m control at the front and back of each day.

Now the original gaps and most of the noise in the RSLE time-series are turned to zero. The zeros are then filled by linear interpolation the get a continuous 365/366-day time-series. The linear interpolation is chosen based on the assumption of a gradually upwards- or downwards- moving snowline in short time e.g. several days.

In this study, the Qilian Mountains is divided into three subregions due to different climate property. For the comparison between the subregions and the whole study domain, the RSLE time-series for a specific domain is obtained as the median of all the RSLE time-series of the tiles in that domain. Considering about the utility in hydrology analysis, the RSLE of the domain is stratified into 100-m elevation zones, Worded differently, the precision of the final RSLE time-series in the subregions is ±100 m.

3.2 Annual number of snow cover days (D_{sc})

Based on the gap-free RSLE time-series, $\mathrm{D_{sc}}$ is estimated in each tile and each year of the 2001-2018 study period. For each pixel in a specific tile on a specific day, the elevation of the pixel is compared with the RSLE of the tile. If the pixel is above the RSLE, it is defined as snow cover; if the pixel is below the RSLE then it is defined as snow-free. For the convenience of the data collection and computation in the Earth Engine, the

period for the estimation of D_{sc} is defined as the calendar year i.e. from January 1st to December 31st, and the total number of the days that the pixel defined as snow cover is D_{sc}.

3.3 Sensitivity of D_{sc} to climatic and topographic factor

3.3.1 The climatic factor

The sensitivity of D_{sc} to climatic and topographic factors is estimated for each elevation zone k in each subregion. The two climatic factors analyzed in this study are precipitation and temperature. To see the spatial and temporal property of these climatic factors, simple statistical analysis is performed.

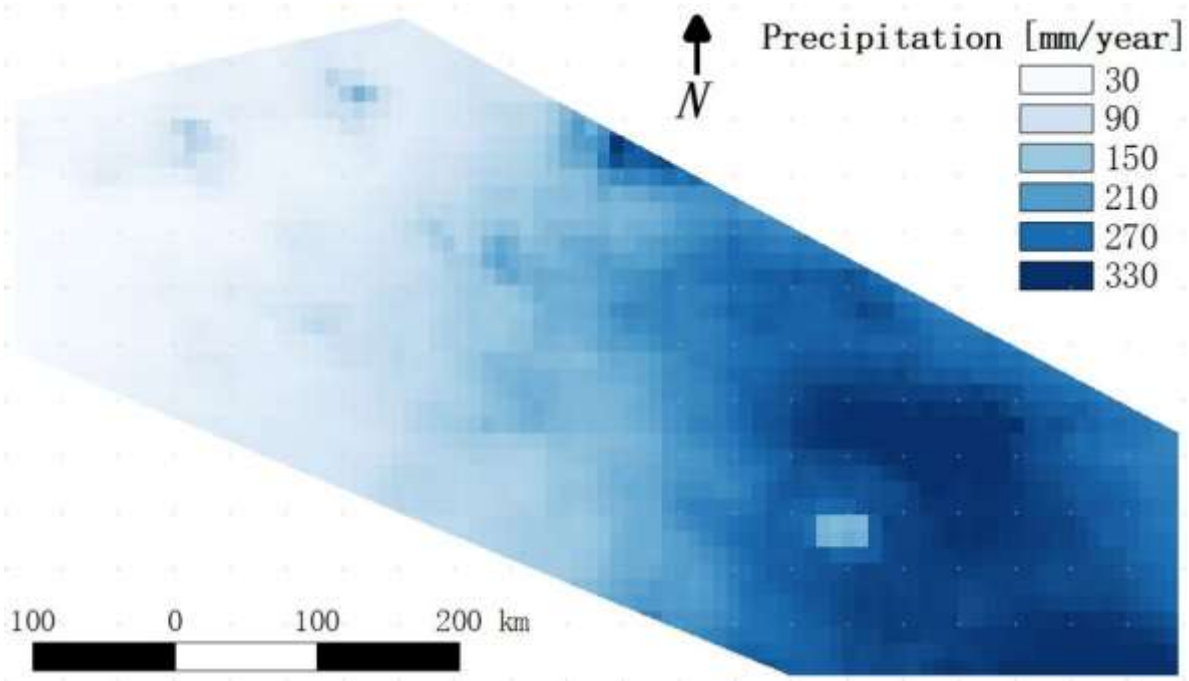

Figure 6. The annual average precipitation from 2001 to 2018

The previous studies (Zhai et al., 2015; Sun et al., 2019) mentioned that the climate of Qilian Mountain is mainly controlled by the monsoons, which leads to a consistency between the temperature and precipitation that high in summer and low in winter. The three subregions of the Qilian Mountains show significantly different climatic characteristics, but all the subregions have dominant precipitation in the warm half-year (from April to September) and rare precipitation in the cold half-year (from January to March, and from October to December).

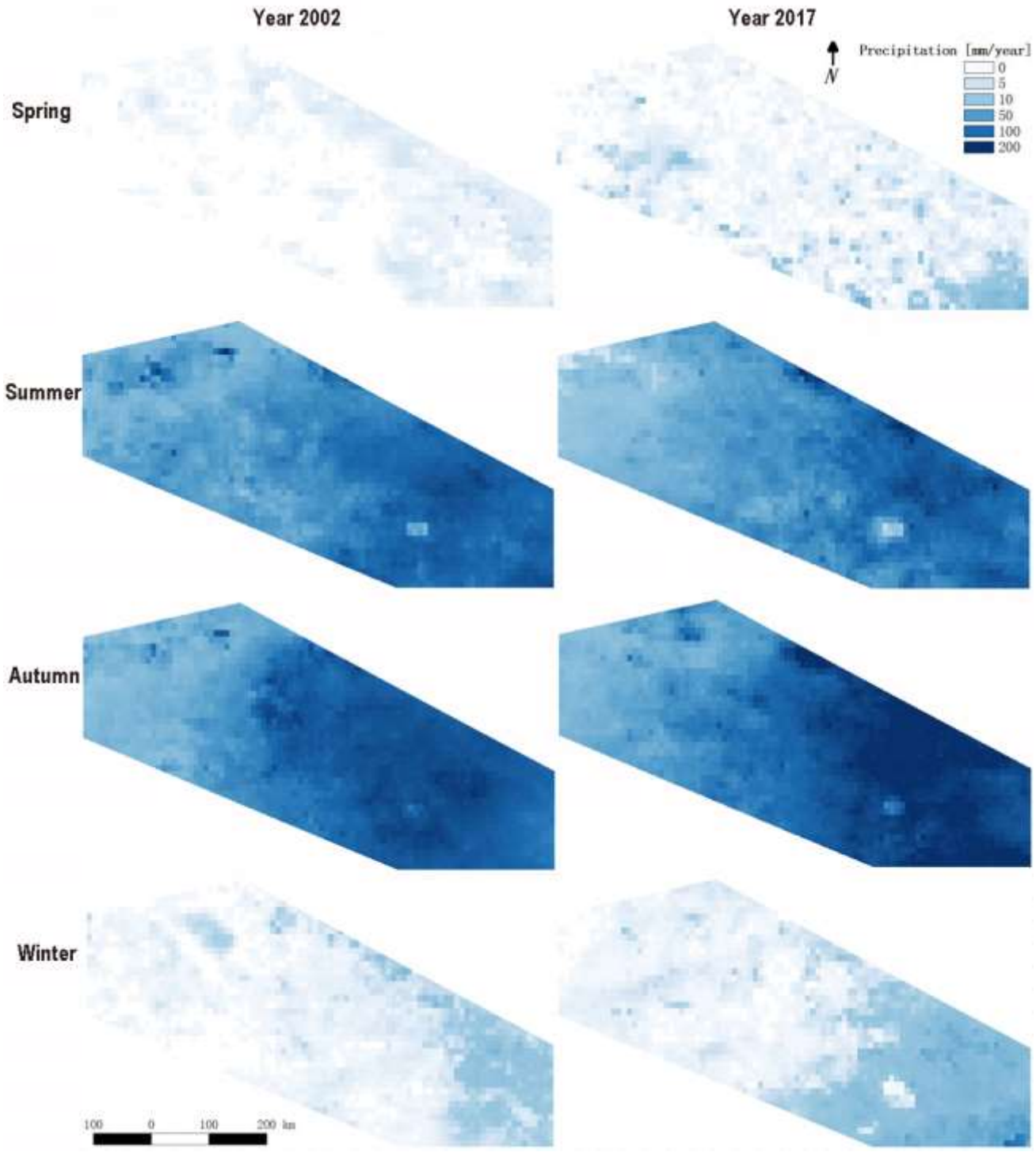

Figure 7. Seasonal accumulated precipitation across the Qilian Mountains in 2002 and 2017

In figure 6 and 7, the results from Global Precipitation Measurement (GPM) show a remarkable spatial distribution that the annual and seasonal accumulated precipitation decrease from west to east. Figure 7 shows a seasonal variation of the precipitation that high in summer and autumn but low in spring and winter and it also indicates that the precipitation in warm half-year is more important than the one in cold half-year for the water supply. Precipitation in the warm half-year is dominant (about 4 times larger than

in the cold half-year) in the Qilian Mountains. Thus, using annual precipitation conceals the connection between cold half-year precipitation and the D_{sc}, and in this study, the sensitivity analysis is based on the cold half-year precipitation instead of annual accumulated precipitation. For the results of analysis based on annual accumulated precipitation, see Appendix A.

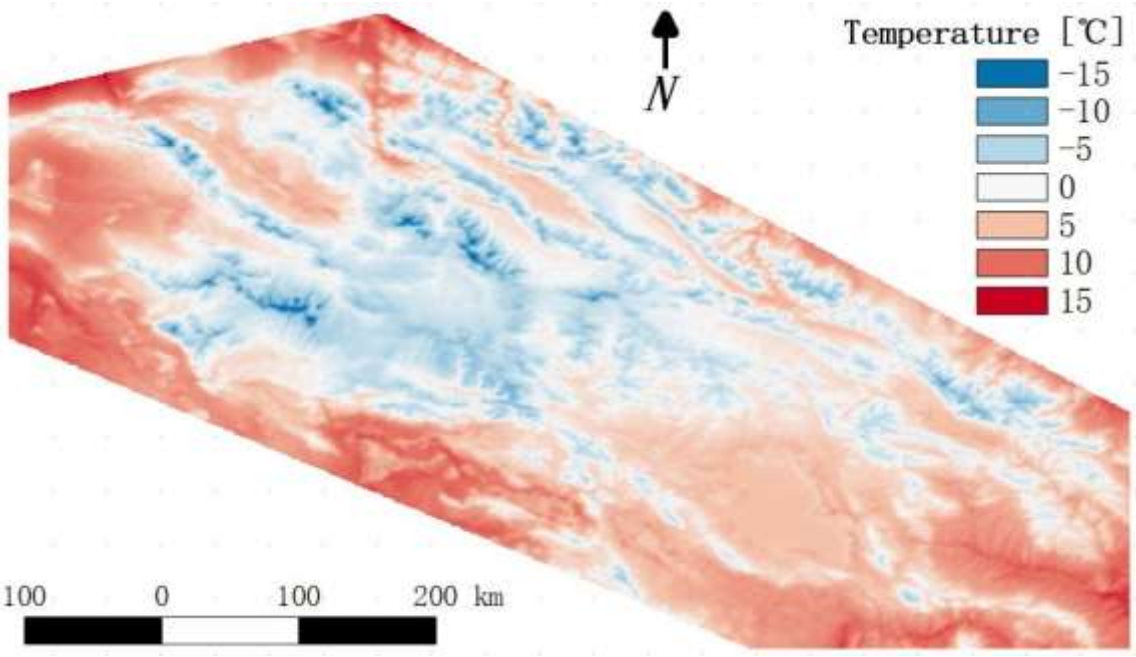

Figure 8. The annual average land surface temperature (LST) from 2001 to 2018

Figure 8 shows the annual average LST low at the mountain and high at the basin and valley. In figure 9, we can see that in the cold half-year the LST of the Qilian Mountains region is mostly below zero. In summer, only the peaks of the mountains i.e. glaciers have their LST below zero, and the below-zero area nearly disappeared in the autumn, especially in the middle section. Considering both the snow melting process in the warm half-year and snow accumulation process in the cold half-year are important to the seasonality of the snow line elevation, the annual average LST is used for the sensitivity analysis in this study.

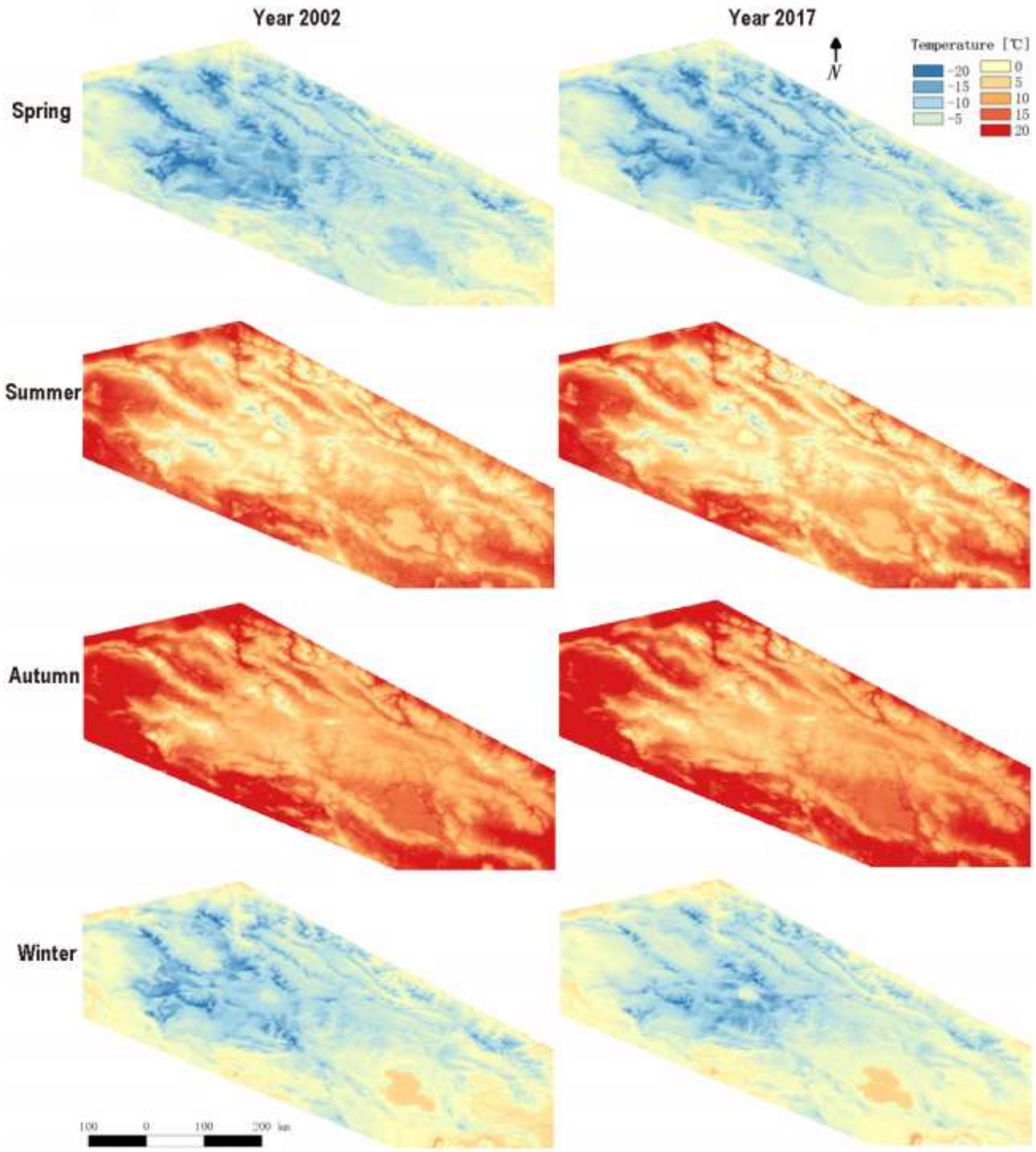

Figure 9. Seasonal average land surface temperature across the Qilian Mountains in 2002 and 2017

As a result, for each year in each subregion, the annual average land surface temperature (T_k) and the accumulated precipitation in the cold half-year ($P_{c,k}$) is extracted from MODIS/Terra MOD11A2 as well as GPM datasets and then related to the individual values of $D_{sc,k}$ from average D_{sc} in the associated elevation zone k. More specifically, three 2-D arrays are built to store the $D_{sc,k}$, T_k and $P_{c,k}$ with the row as time direction in the one-

year interval and the column as elevation direction in the 100-meter interval. In order to understand the variability of the relative importance of T_k and $P_{c,k}$ as predictors of $D_{sc,k}$, the linear relationship is hypothesized of $D_{sc,k}$ with T_k and $P_{w,k}$ to analyze their individual explanatory power, respectively. Besides the simple linear regressions, a multivariate linear regression of the To climatic variables i.e. T_k and $P_{c,k}$ is applied in the form of $D_{sc,k} = F(T_k, P_{c,k})$.

Different numbers of predictors can be explained by using the adjusted R-squared indicator (Theil,1961). The individual sensitivity of $D_{sc,k}$ to annual average temperature T_k and cold half-year accumulated precipitation $P_{c,k}$ is defined as the variance in $D_{sc,k}$ per change in T_k and $P_{c,k}$, respectively. If $P_{c,k}$ is related to T_k, and any of them are individually related to $D_{sc,k}$ in a naive approach, $D_{sc,k}$ will have spurious sensitivities to both T_k and $P_{c,k}$. To consider the influence of possible correlation between T_k and $P_{c,k}$, assuming the possible correlation between T_k and $P_{c,k}$ is linear, the sensitivity of $D_{sc,k}$ to either of them is corrected by:

$$\varepsilon_{T,k} = \frac{\partial D_{sc,k}}{\partial T_k} = \frac{dD_{sc,k}}{dT_k} - \frac{\partial F(T_k,P_{c,k})}{\partial P_{c,k}} \frac{dP_{c,k}}{dT_k} \quad [\text{day}/℃] \tag{6}$$

$$\varepsilon_{P,c,k} = \frac{\partial D_{sc,k}}{\partial P_{c,k}} = \frac{dD_{sc,,k}}{dP_{c,k}} - \frac{\partial F(T_k,P_{c,k})}{\partial T_k} \frac{dT_k}{dP_{c,k}} \quad [\text{day}/(\text{mm}/\text{year})] \tag{7}$$

where $\varepsilon_{T,k}$ and $\varepsilon_{P,c,k}$ are the sensitivities of $D_{sc,k}$ to T_k and $P_{c,k}$, respectively. The derivatives are Theil-Sen's estimates of the slope terms. The two equations above are applied along the row (time) direction and column (elevation) direction for the arrays.

Through the spatial discretization and elevation stratification of the sensitivities $\varepsilon_{T,k}$ and $\varepsilon_{P,c,k}$, respectively, we can not only characterize their temporal variabilities across the years but also identify the elevation-related changes of the two individual sensitivities. Additionally, the two individual sensitivities are analyzed to obtain a spatial pattern to find if in any of the subregions the potential changes in one or two climatic variables may have a greater impact on $D_{sc,k}$.

3.3.2 The topographic factor

In addition to the clouds, the combination of the effects of solar incident angles and

topographic shading i.e. hillshade is the first-order controls on direct solar radiation. Direct solar radiation is a key component of the energy balance on the ground surface, and thus it also plays an important role in snow accumulation and melting dynamics. In this study, the hillshade is set to be the representation of direct solar radiation. A hillshade is a grayscale 3D representation of the surface, with the sun's relative position (elevation and azimuth) taken into account for shading the image.

To understand the effect of the hillshade on D_{sc}, the average annual D_{sc} from 2001 to 2018 is related to the hillshade value in the three subregions and the whole Qilian Mountains region. The analysis is based on the hillshade map generated with the 'Hillshade function' in GEE or ArcGIS (which share the same method). By default, shadow and light are shades of gray associated with integers from 0 to 255, and for more detail of the function, the reader is referred to the ArcGIS manual. To discover the correlation between D_{sc} and hillshade, the hillshade map is split based on the hillshade value with 1 as interval and for each hillshade value, the mean value of the average annual D_{sc} map is calculated.

3.3.3 Temporal evolution of D_{sc}

In addition to the above-mentioned spatial estimation of the sensitivities of D_{sc} to inter-annual climate changes i.e. $\varepsilon_{T,k}$ and $\varepsilon_{P,c,k}$, we analyzed the actual observed temporal evolution of D_{sc} caused by the interaction between the climate variables throughout the entire the Qilian Mountains over the study period. The Mann-Kendall trend test, as well as other statistical analyses including theil-sen's slope and standard deviation, are performed on the annual D_{sc} time-series, the annual average land surface temperature (T) and the cold half-year accumulated precipitation (P_c) across the study domain to find the regions where D_{sc} changed significantly during the study period and if T and/or P_c also changed significantly in these areas. Although in principle D_{sc} in a certain area may be sensitive to climatic forcing changes of $\varepsilon_{T,k}$ and $\varepsilon_{P,c,k}$, respectively, the magnitude of changes in climate variables during the study period may be too small and/or may offset each other, which finally result in only small variations in D_{sc}.

4 Results

4.1 Regional snow line elevation (RSLE)

Figure 10, comparing to figure 5, has changed many snow-free pixels into snow-covered. In four specific days (January 1st, April 1st, July 1st, and October 1st) in the two selected years (2002 and 2017), RSLE estimates for the entire the Qilian Mountains show significant regional differences. While the spatial pattern of RSLE generally follows the undulations of the topography, the regional differences between the three subregions of the Qilian Mountains have become apparent. Although the snapshots are timely, figure 10 shows that the average RSLE in the east section is lower than the one in the west and middle section, and figure 11 gives the same result.

Even though the daily RSLE varies a lot in all subregions, figure 11 shows that the RSLE in the subregion has raised about 100-200 m in July and August in the study period. It is clear that the east section is always around 300 meters lower than the west at the same time in the same year. The RSLE in the middle section is as low as east in the winter and as high as west in the summer, and thus has a larger variability in the year. The highest RSLE in the east, middle and west are 4700, 4800 and 5000 m.a.s.l, respectively, and the highest point is always from July to August. For all the subregions, the maximum inter-annual difference of the RSLE is in the 1000-1500 m.a.s.l range. Moreover, the RSLE time-series is more smooth in the west subregion, with an earlier starting time of snow melting (in March) and a later starting time of snow accumulation (in October). The start of snow melting and snow accumulation, in the east and middle subregions, are April and September, respectively. This regional difference possibly due to the difference of interaction between the precipitation and land surface temperature, which will be discussed later.

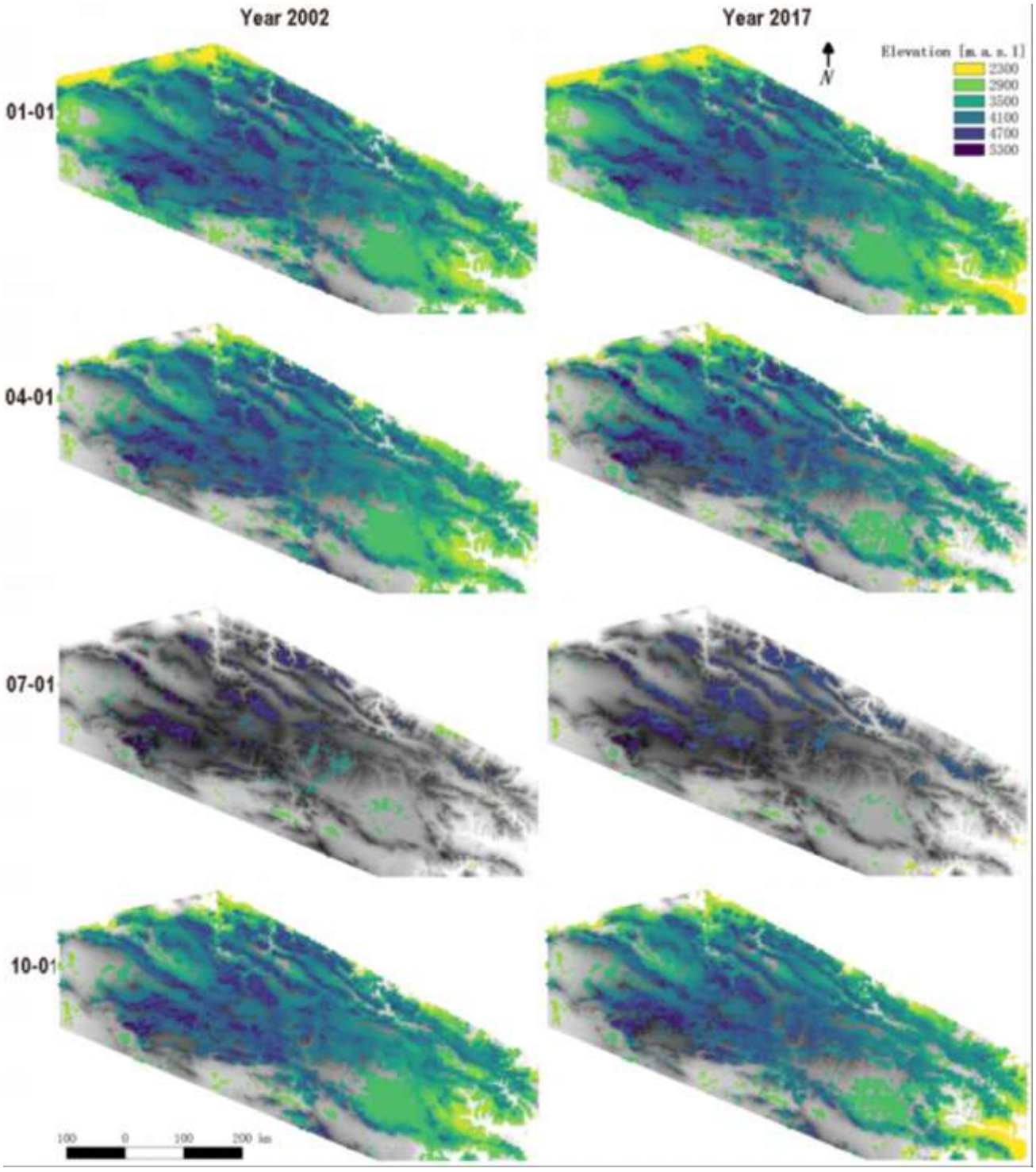

Figure 10. Gap filled RSLE across the Qilian Mountains on January 1st, April 1st, July 1st, October 1st for the year 2002 and 2017

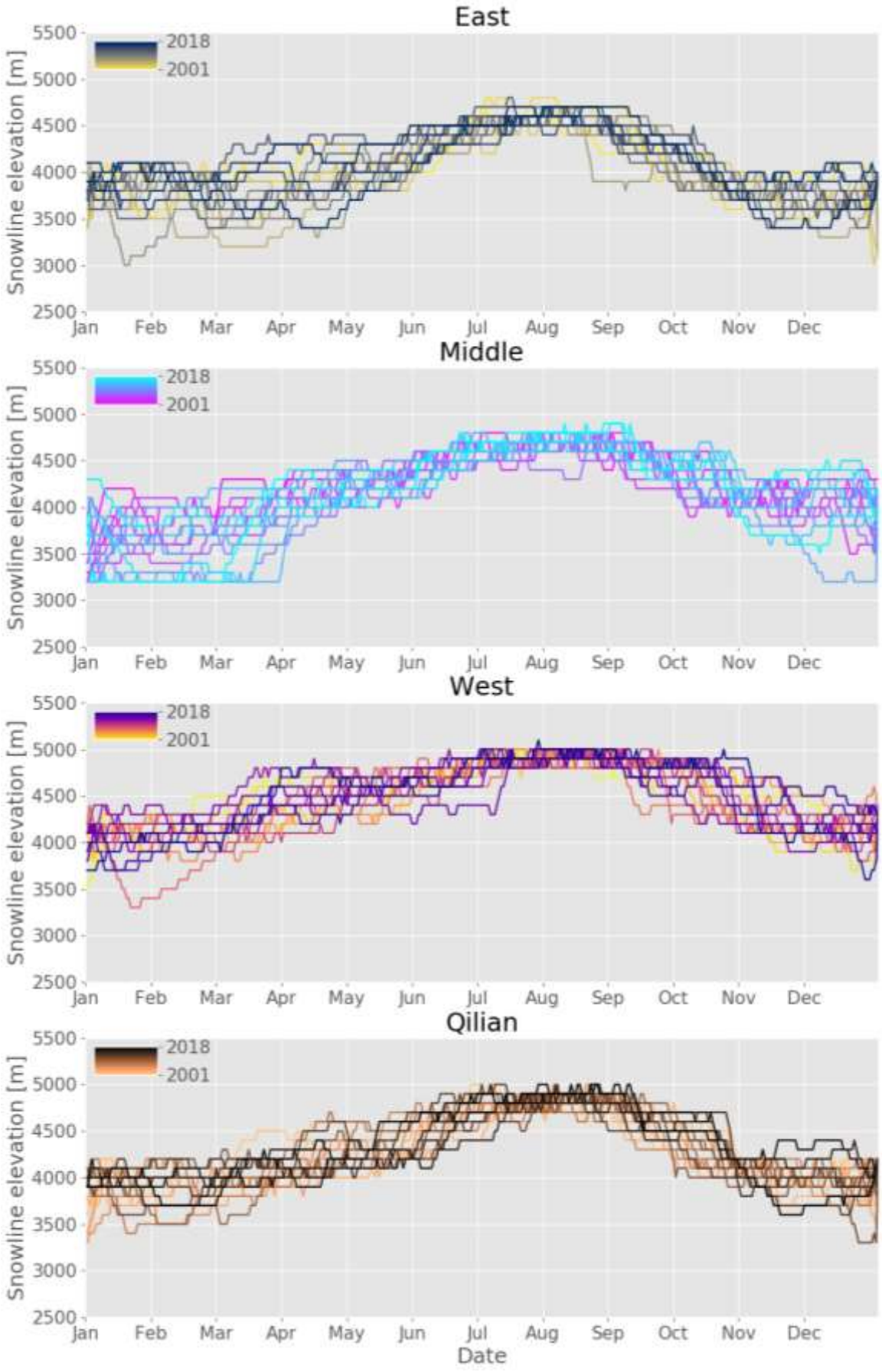

Figure 11. The estimated daily snowline elevation for subregions and the entire Qilian Mountains region from 2001 to 2018 (in 100-meter precision)

4.2 Spatial distribution of annual number of snow cover days

The above-mentioned inter-annual spatial variability in RSLE directly translates into significant local and regional differences in D_{sc}. Figure 12 shows the spatial distribution of the average number of annual snow cover days D_{sc} for the period from 2001 to 2018. Across the Qilian Mountains, most of the regions have a D_{sc} lower than half a year i.e. only in cold half-year, while some consistent glaciers are located at the peaks of the mountains.

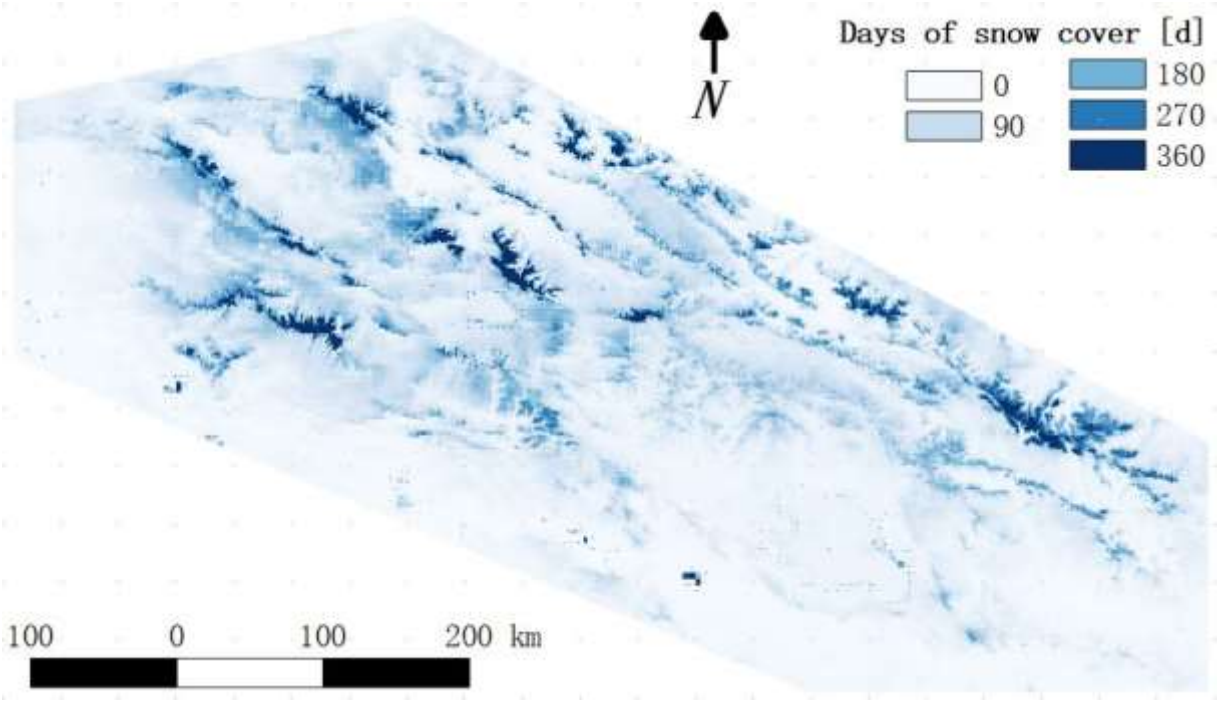

Figure 12. The annual average snow cover days (D_{sc}) from 2001 to 2018

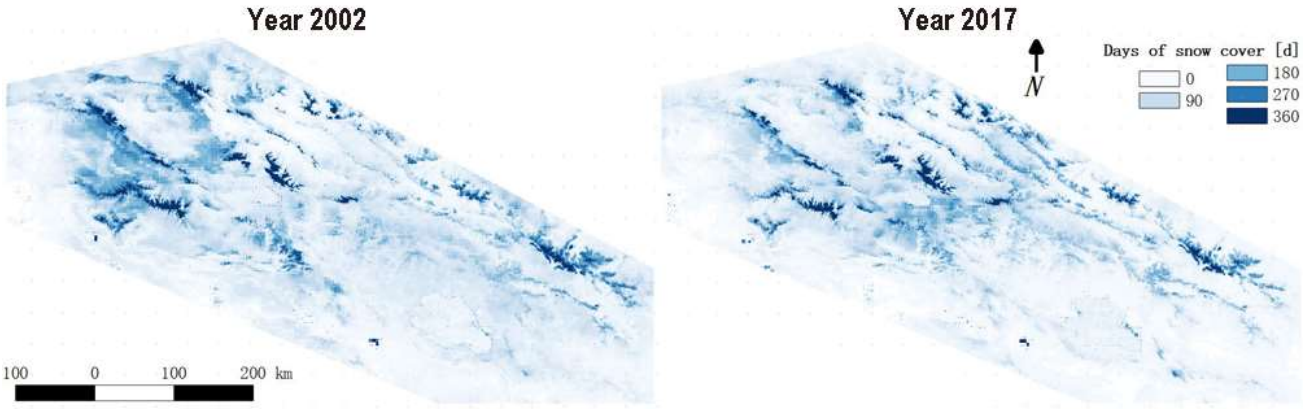

Figure 13. The annual average snow cover days (D_{sc}) in 2002 and 2017

The south-east region is the low-elevation area (about 3000 m.a.s.l) around the Qinghai Lake and thus has very low D_{sc}. D_{sc} at the edges of the study region are also very low because of the low elevation. In the north belt-like area, some parallel lines with large D_{sc} go from north-west to south-east, which corresponds to the parallel mountain branches in the topography. In figure 13, it is clear that D_{sc} at the margin of the mountain peaks (at 4000-5000 m.a.s.l) i.e. glaciers in the Qilian Mountains has decreased in 2017 compared to 2002.

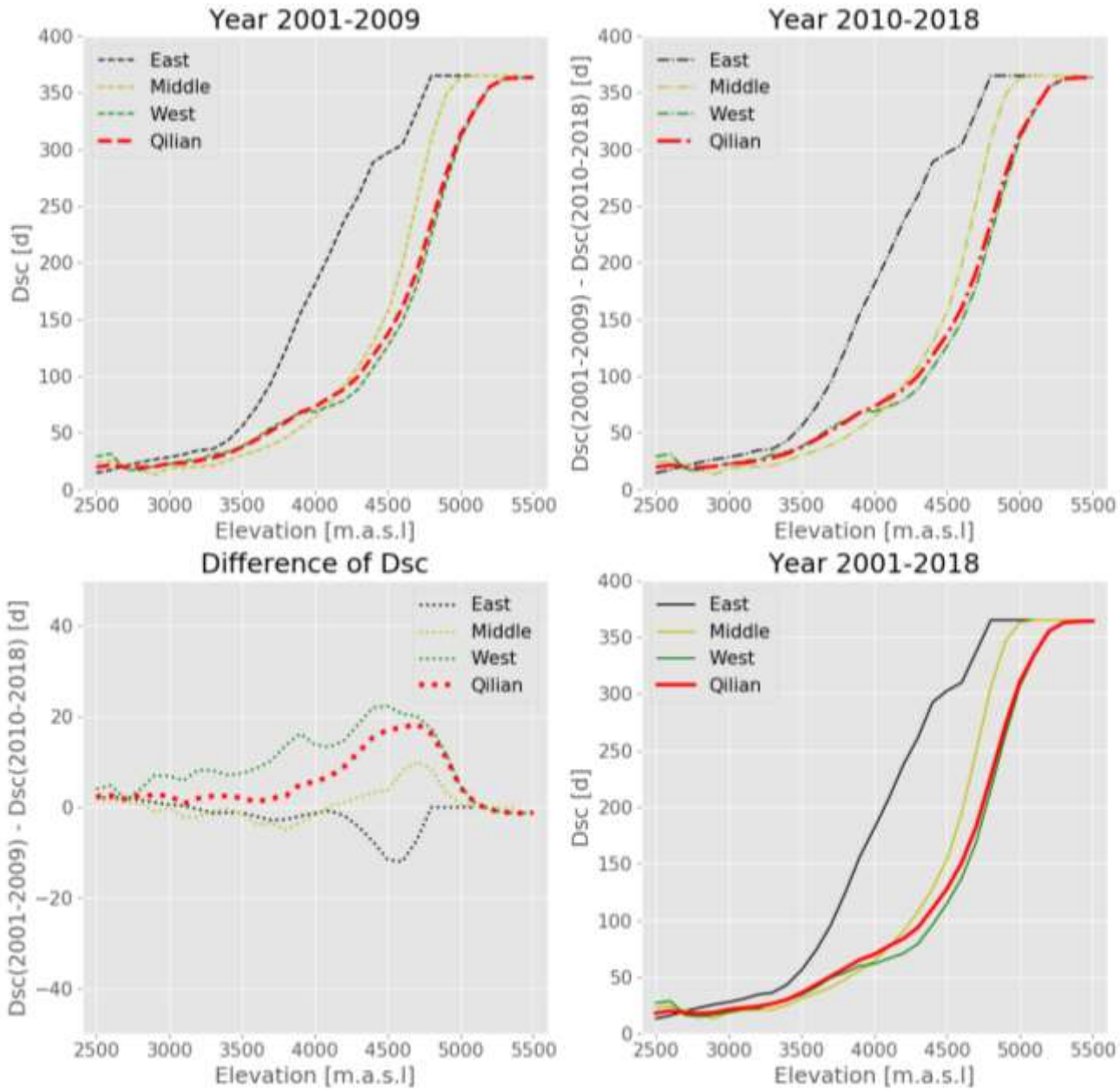

Figure 14a. The average D_{sc} against elevation curve for different regions in year 2001-2009, in year 2010-2018, in year 2001-2018, and the difference between year 2001-2009 and year 2010-2018.

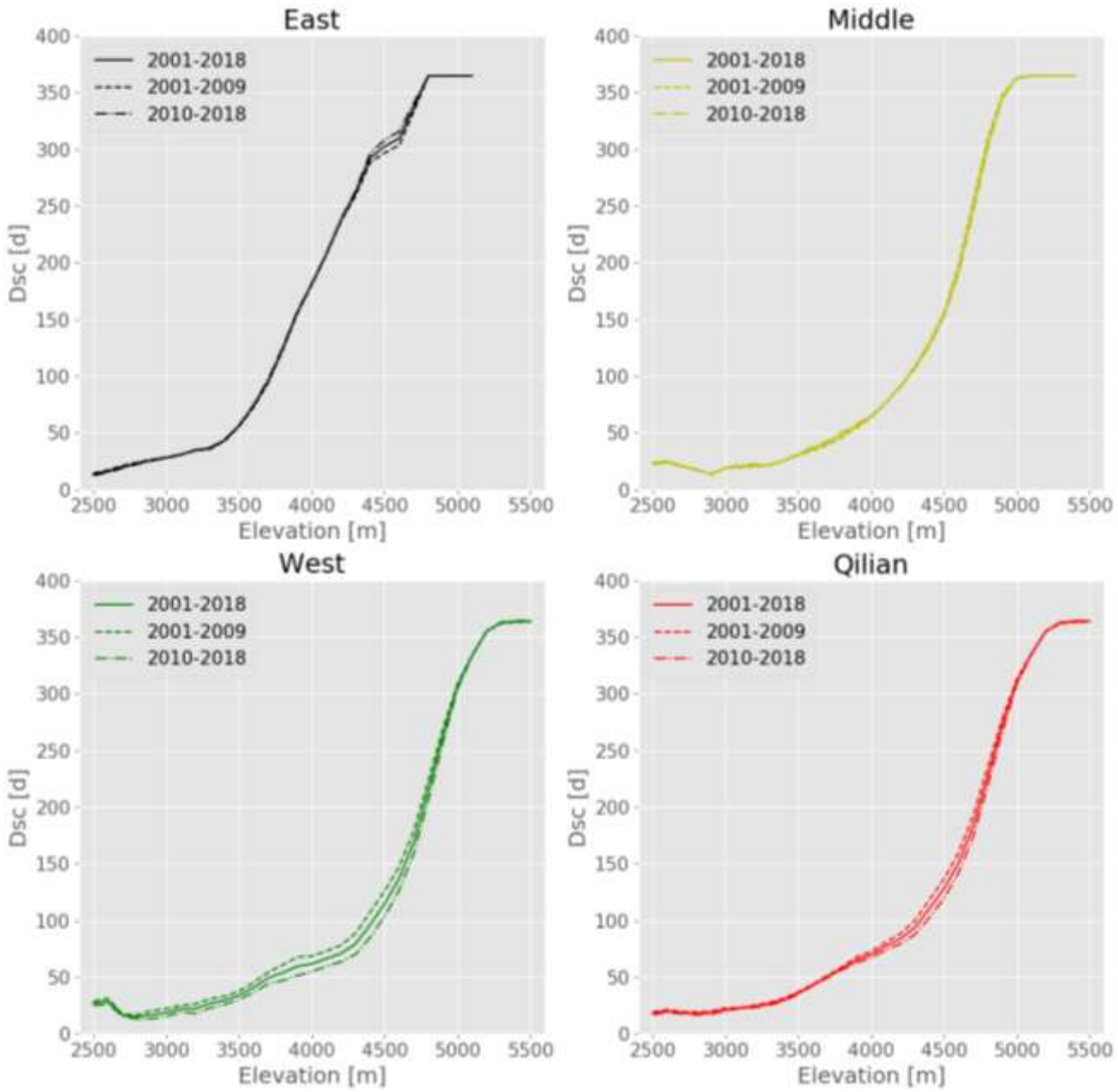

Figure 14b. The average D_{sc} against elevation curve for different time periods in each subregion and the whole Qilian Mountains region

Remarkable differences of D_{sc} among the subregions in different periods i.e. the year 2001-2009 and the year 2010-2018 are shown in figure 14a and 14b. In all the periods shown in figure 14a, the east subregion has a higher D_{sc} at the same elevation but also a lower elevation of the glacier, comparing to the other subregions. The middle section, compared to the west section, has a lower D_{sc} at the low elevation i.e. 3000-4000 m.a.s.l, but a higher D_{sc} at higher elevation. The property of D_{sc} in the entire Qilian Mountains is very close to the one in the west sections. Figure 14a also indicates that D_{sc} in the middle and west subregions has decreased, while in the east subregion D_{sc} has

increased. The sharpest change of D_{sc} appears at the regions with an elevation around 4500 m.a.s.l, with about 20 days decreasing in the west, about 10 days decreasing in the middle, and about 15 days increasing in the east. In figure 14b, the west subregion has its D_{sc} decreased from 3000 to 5000 m.a.s.l in the past years. Across the entire Qilian Mountains, D_{sc} is about 20-40 days at elevations below 3500 m.a.s.l and increases to about 130 days at 4500 m.a.s.l, and more than 300 days above 5000 m.a.s.l. In the west, D_{sc} is always lower than the east at the same elevation, and the largest difference is about 200 days at 4300 m.a.s.l. The middle subregion has its D_{sc} lower than the west below 4000 m.a.s.l, but higher above that elevation.

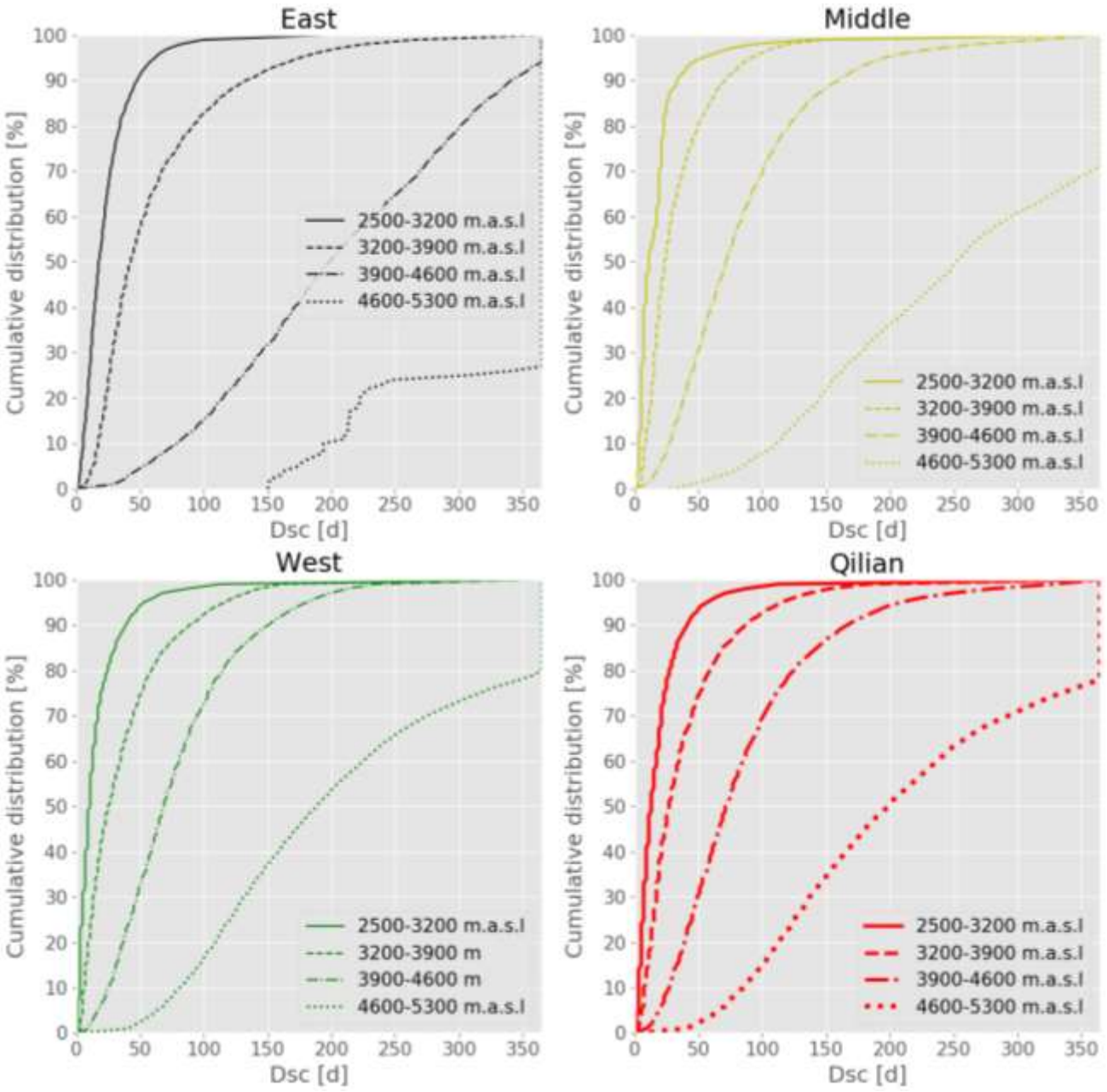

Figure 15a. Cumulative distribution of D_{sc} aross elevation in subregions and the Qilian Mountains

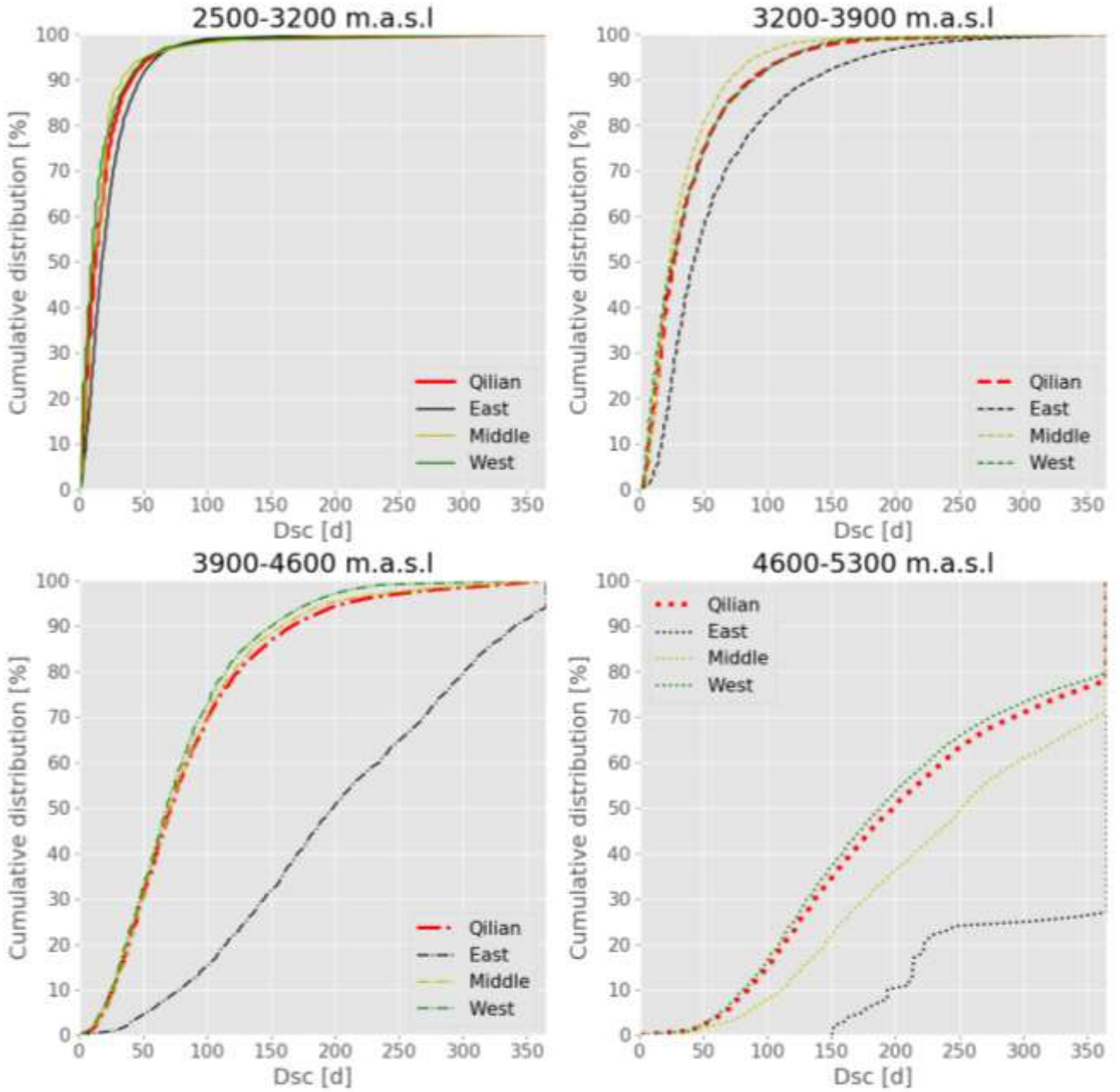

Figure 15b. Cumulative distribution of D_{sc} in different regions in 2500-3200, 3200-3900, 3900-4600, and 4600-5300 m.a.s.l regions

The same spatial pattern of D_{sc} is also found in figures 15a and 15b. The cumulative distribution curves of D_{sc} against different 700-m elevation zones in figure 15a is similar in the west and middle section, though the CDF of the middle section in 4600-5300 m.a.s.l is more straight and reaches the glacier point (365 days) earlier at 70%, while the CDF in the west reaches the glacier point at 80%. Again, we find the west section is dominant in the Qilian Mountains region by comparing the sub-figures. The east section shows very different curves with a relatively high D_{sc} at the same CDF percentile above 3900 m.a.s.l, and reaches the glacier point much earlier, which suggests that the glaciers in the east

subregion have a lower elevation than the other subregions. In figure 15b, the regional difference of D_{sc} is small at the low-elevation region i.e. 2500-3200 m.a.s.l, and the difference is enlarged when the elevation increase.

4.3 Temporal evolution of D_{sc} and the climatic factors

4.3.1 Evolution of annual snow cover days

Through comprehensive statistical analysis across the entire the Qilian Mountains, we can understand the distribution of major changes in D_{sc} from 2001 to 2018. From the result of Kendall tau-b and Theil-Sen's slope, the D_{sc} has an increasing trend no more than 1 d/year at some regions in the middle and east sections, and most of the west section has a decreasing trend up to -5 d/year. The north-east part of the Qilian Mountains also has decreasing trend of D_{sc}.

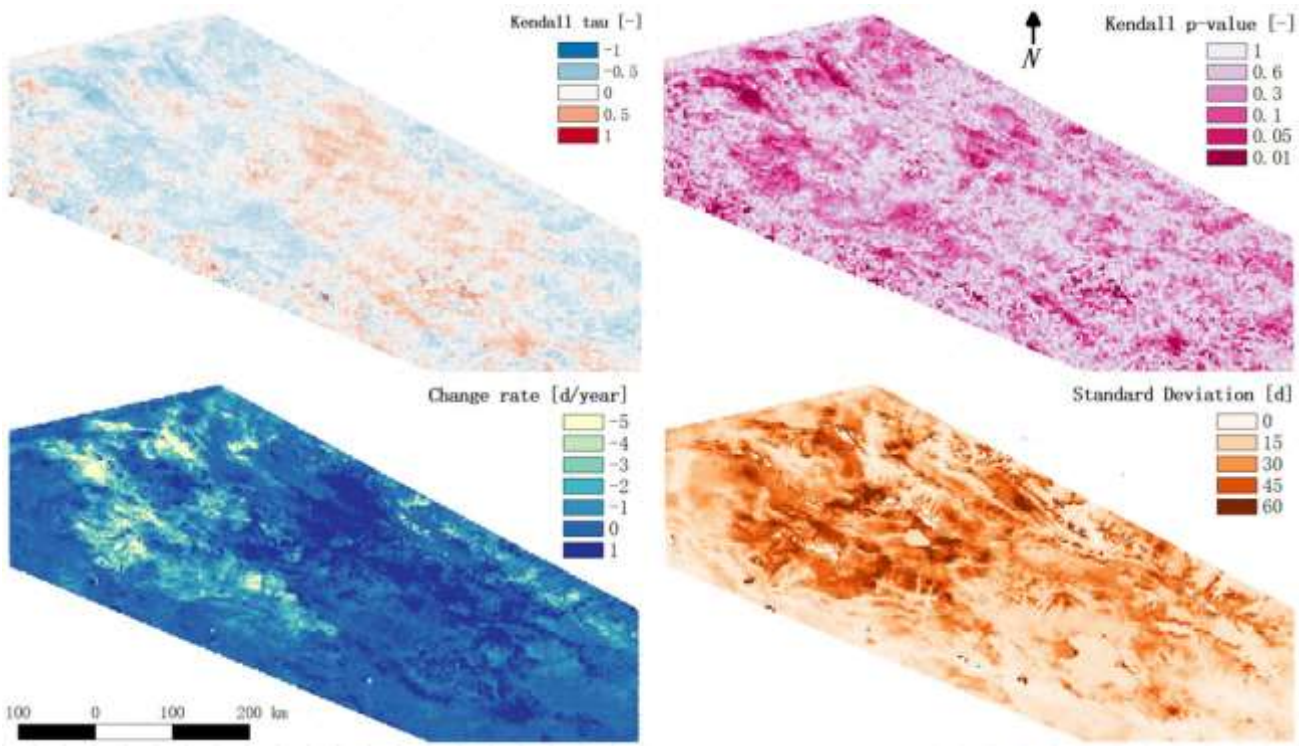

Figure 16. Kendall rank correlation coefficient tau-b, Kendall p-value, standard deviation, Theil-Sen's slope for the trend of the number of annual snow cover days D_{sc} from 2001 to 2018

However, only a few regions has a Kendall p-value below the significant level i.e. 0.05, which suggests that the emergence of the trend in most of the Qilian Mountains region is irrelevant to the temporal evolution, and it is supported by the standard deviation map

where the southern hillsides have a much higher standard deviation (more than 45 days) than the basin region. Furthermore, we can find some regions where significantly snow cover decline appears. In the west subregion of the maps, some areas at 3500-4500 m.a.s.l have a confident D_{sc} change rate around -5 d/year with a p-value under 0.05. If the significant level threshold of the p-value is increased to 0.1, most of the areas with a decreasing trend from -3 to -5 d/year can be considered as confident, and the increasing trend at some low-elevation regions in the middle and east will be confident too.

4.3.2 The climatic factors

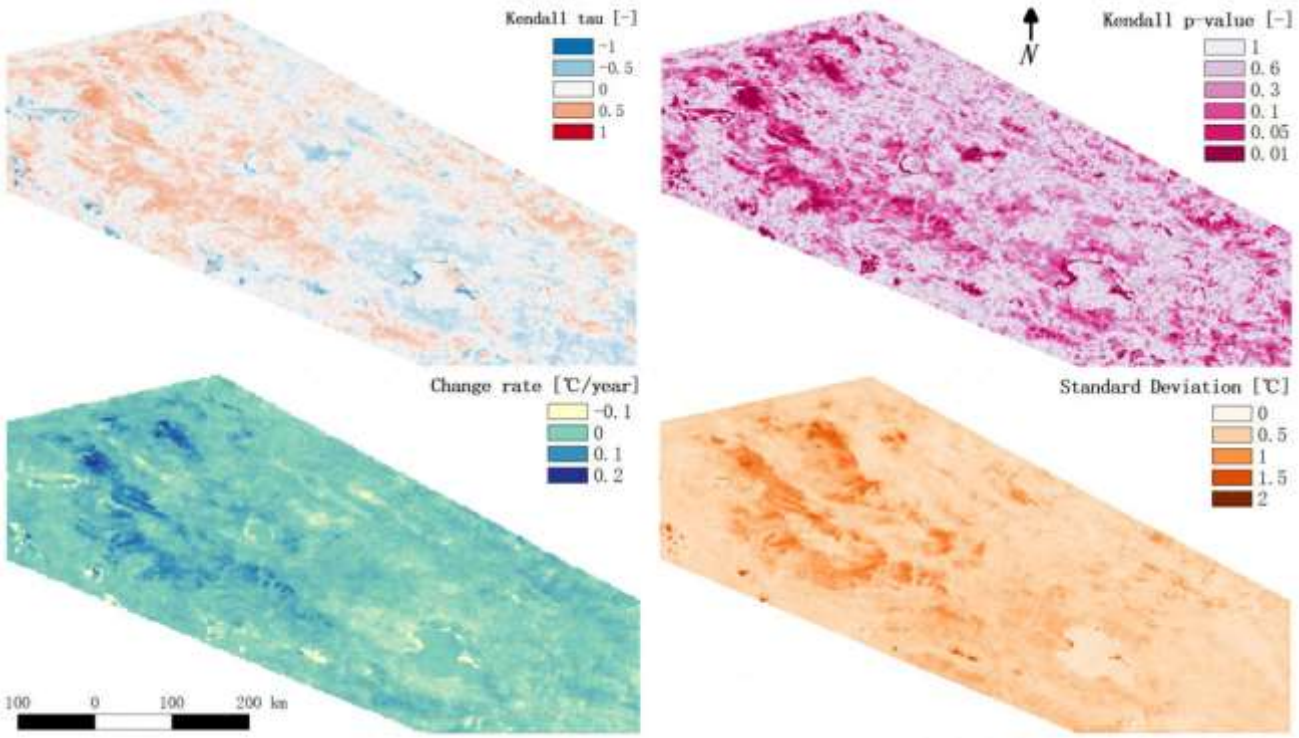

Figure 17. Kendall rank correlation coefficient tau-b, Kendall p-value , standard deviation , Theil-Sen's slope for the trend of the annual average land surface temperature T from 2001 to 2018

The land surface temperature and winter half-year precipitation trends are analyzed and considered separately. For the annual average LST (figure 17), like the analysis of D_{sc}, the Kendall tau-b value and p-value, and Theil-Sen's slope, together with show some significantly varying regions on the map, while the other areas are much less important. The 'warming region' with more than 0.1 °C increase per year is mostly located at the west subregion, which is exactly the location of the decreasing trend taht appears in the

D_{sc} map. The standard deviation map suggests that the temperature varies a lot with a deviation of more than 1 °C on the hillsides in the west subregion.

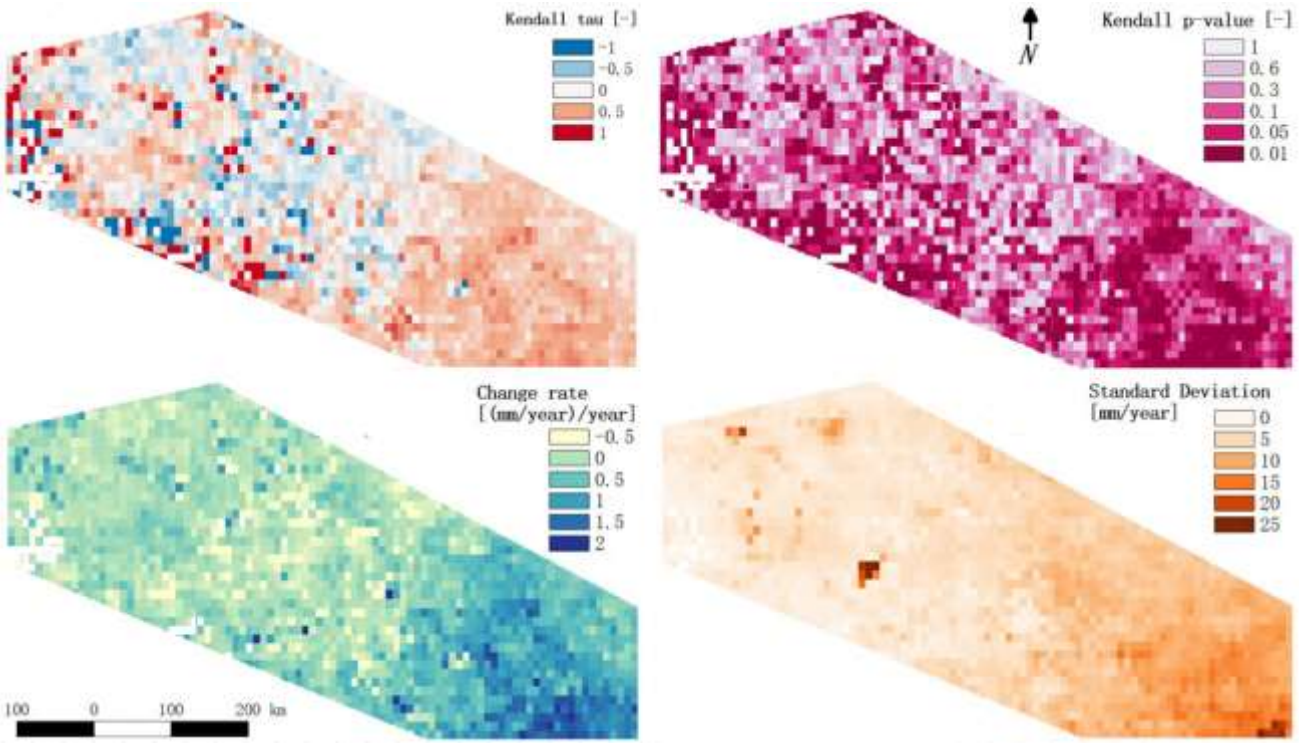

Figure 18. Kendall rank correlation coefficient tau-b, Kendall p-value , standard deviation, Theil-Sen's slope for the trend of the winter half-year (January to March, and October to December) precipitation P_c from 2001 to 2018

The trend of cold half-year accumulated precipitation (figure 18) shows a spatial pattern that the precipitation only increases in the east with rates of more than 1 mm/year. the standard deviation map gives the same result with the south-east corner has the highest deviation for more than 15 mm/year. However, the region with an extremely high standard deviation (about 25 mm/year) may come from special local characteristic e.g. vegetation and human activity, since the elevation and temperature are this region is not very different from its neighbors.

4.3.3 Relating D_{sc} to temperature and precipitation

Continuing the combined analysis of D_{sc} with T and P_c, the tiles are grouped by climate subregion and the linear regression is performed. Throughout the elevations (figure 19), the sensitivities show that $P_{c,k}$ has weak effects in the east and middle subregions, but

relatively strong positive effects (more than 6 d/(mm/year)) at 3500-4500 m.a.s.l in the west and near the 4500 m.a.s.l in the entire the Qilian Mountains. T_k has consistent negative effects on $D_{sc,k}$ at all elevations in all subregions, but the maximum sensitivity is at 4000 m.a.s.l in the east (about -40 d/℃), and at 4000-4500 m.a.s.l. in other regions (from -30 to -40 d/℃). The result of R-square shows a spatial difference across the subregions, that the R-square of $P_{c,k}$ in the east subregions is smaller than 0.2, in the middle it increases to 0.4 as maximum, and in the west, the maximum R-square of $P_{c,k}$ is more than 0.5. The maximum R-square of $P_{c,k}$ appears between 4000 and 4500 m.a.s.l. The maximum R-square of T_k is around 0.4, 0.5, 0.6 at 4000, 4500-5000, 5000 m.a.s.l in the east, middle, west subregions, respectively.

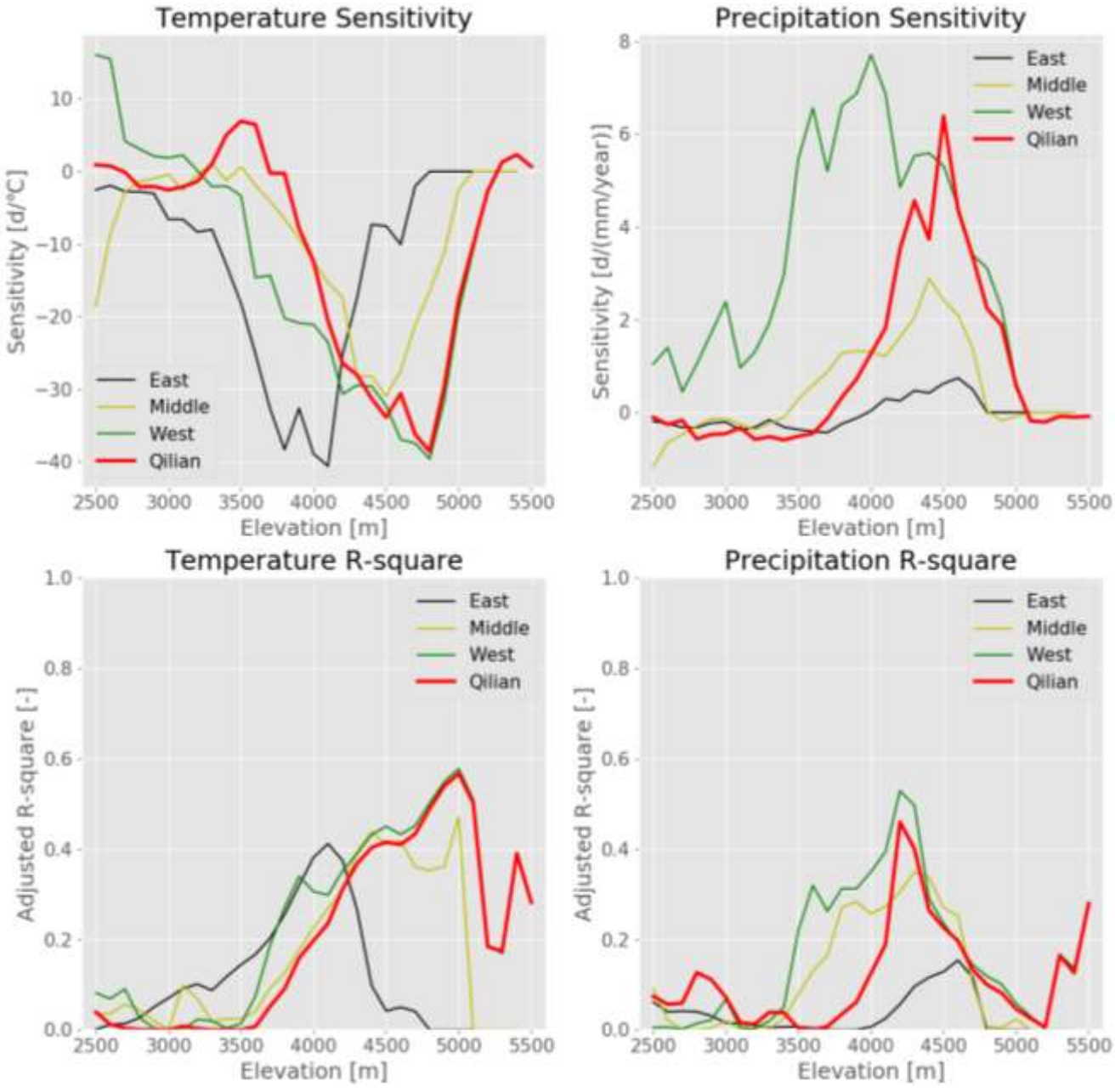

Figure 19. The sensitivity and R-square of the D_{sc} to temperature and cold half-year accumulated precipitation through different elevations in each subregion and the Qilian Mountains region

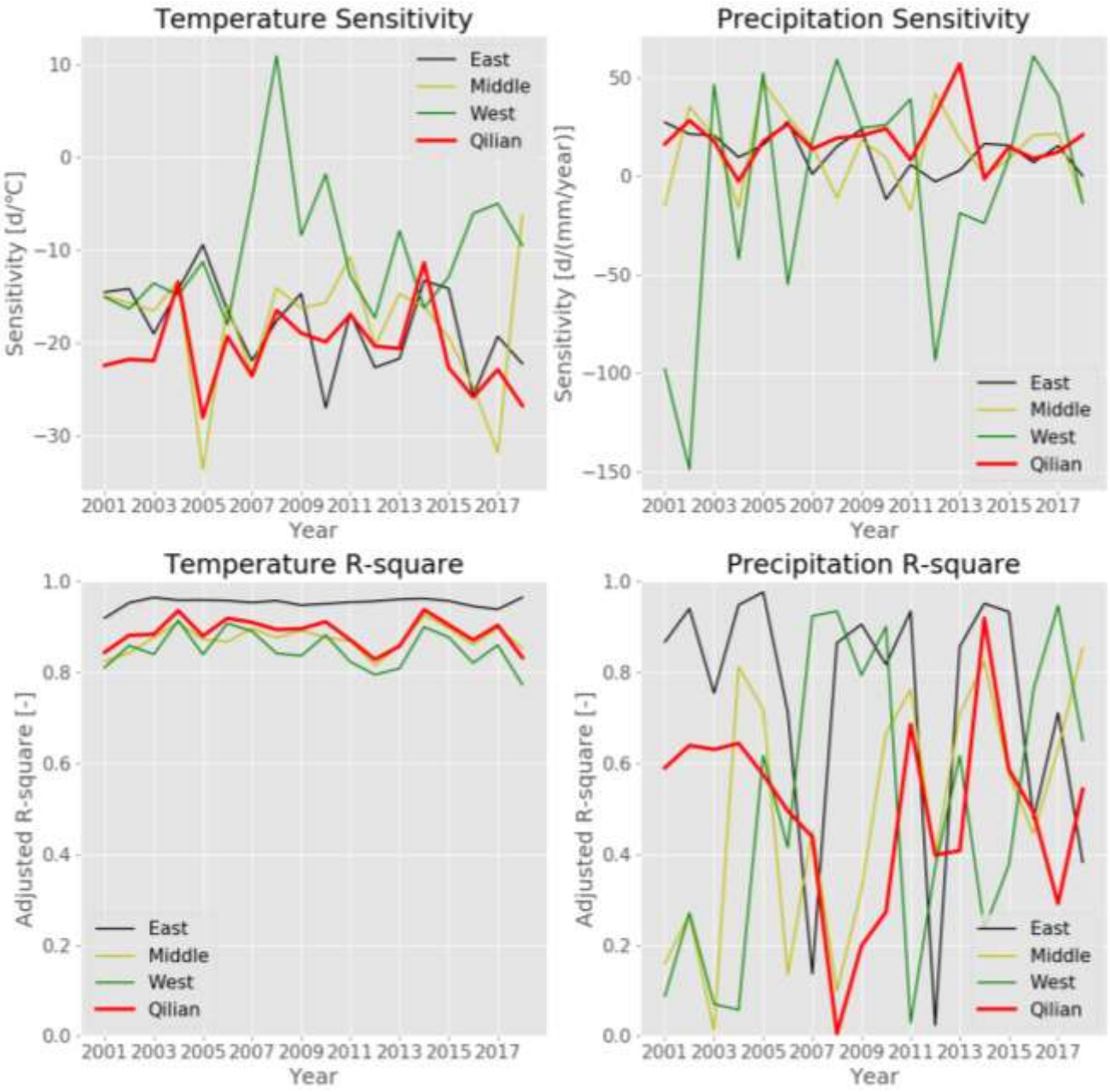

Figure 20. The sensitivity and R-square of the D_{sc} to temperature and cold half-year accumulated precipitation through different years in each subregion and the Qilian Mountains region

Across the 18 years (figure 20), the effects from $P_{c,k}$ are very unstable and only the east section seems to have a confident positive effect from $P_{c,k}$ across the years. The negative effects of T_k are consistent and strong (about -20 d/℃) except in the west, where T_k has to have positive effects from 2007 to 2010. The R-square of $P_{c,k}$ randomly changes much in the study period, which indicates that the temporal evolution of $D_{sc,k}$ may have little connection with the individual variation of $P_{c,k}$; the R-square of T_k is

always greater than 0.8 in each subregion and that highlight the correlation between land surface temperature and D_{sc}.

4.4 Relating D_{sc} to hillshade

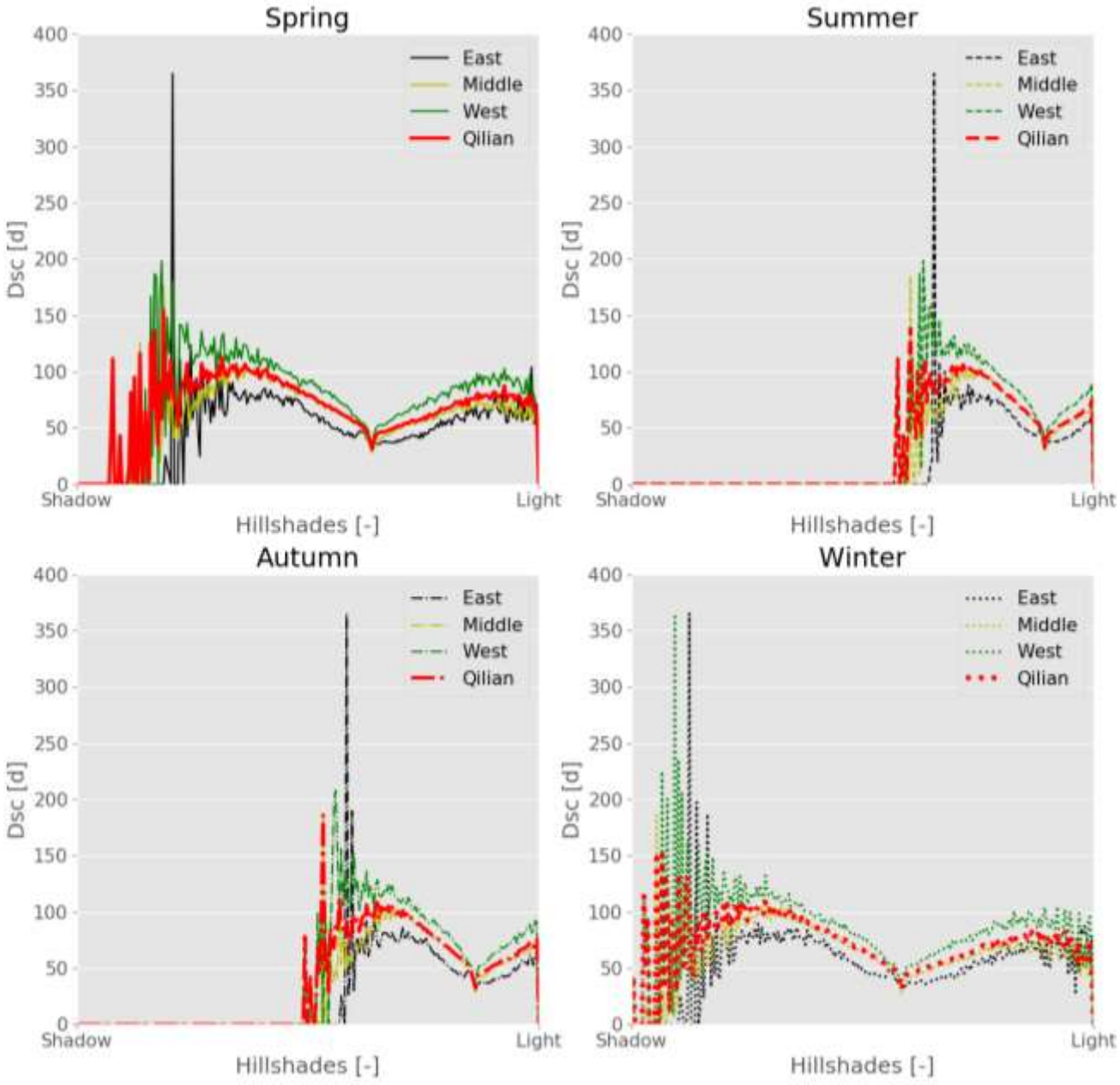

Figure 21. For each season, the correlation between hillshade and the average number of annual snow cover days in 2001-2018 period

The correlation between average D_{sc} and hillshade across the region is interesting. In figure 21, we can see that hillshade moves to the shadow side in spring and winter, and moves to the light side in summer and autumn (also in Appendix B). Additionally, shadow regions always have the highest D_{sc}, and D_{sc} keeps decreasing until a specific point of

hillshade which depends on the season. After that point, D_{sc} increases as the hillshade becomes lighter. This phenomenon that the lighter hillshade has higher D_{sc} may be explained with figure 22. Figure 22 shows that the hillshade with the maximum area in the subregions are very close to the hillshade at the low point of D_{sc} in figure 21, and it means that, the lightest hillshade areas are more likely to be high peaks of the mountains i.e. glaciers, while the medium hillshade areas are more likely to be hillsides at the low or medium elevation. So the average D_{sc} in the lightest hillshade is higher than the one with medium hillshade.

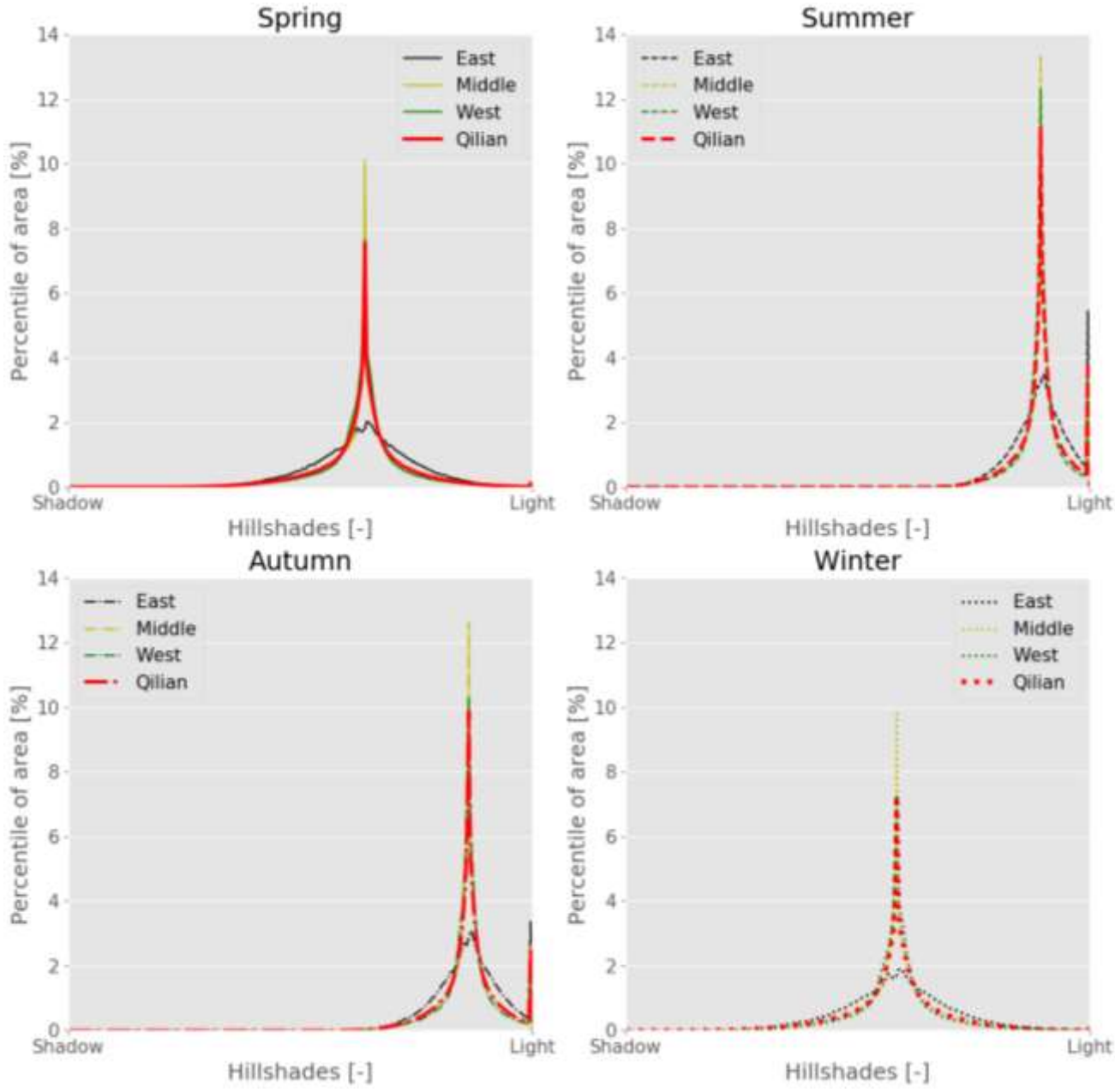

Figure 22. For each season, the average percentiles of the area of different hillshade in 2001-2018 period

5 Discussion

Our goal of using the combination of the RSLE method and MODIS snow products is to derive the spatial and temporal snow cover pattern in the Qilian Mountains, especially the regional variability in the study period i.e. from 2001 to 2018. This goal is achieved by applying the adjusted RSLE method on a multi-catchment spatial scale to get the resulting RSLE time-series. D_{sc} calculated from the RSLE time-series is used as our quantification of snow cover duration. The regional trend of D_{sc} during the study period is linked with the climate variables T and P_c whose trend is also established and analyzed. Besides, the potential correlation between the topography i.e. hillshade and D_{sc} is discovered.

5.1 Regional snow line elevation

As mentioned in the introduction, various studies have been done on the snow line elevation and snow cover frequency in the Qilian Mountains (e.g. Zhang et al., 2005; Han et al., 2011; Guo et al., 2003; Wang et al., 2010), but mostly on a basin scale. Combining these studies, we can find that the characteristics of the snow line in the subregions of the Qilian Mountains are different, that the west section has a higher snow line elevation than the east section, and during the past decades, the snow line elevation has raised.

In this study, we determine the RSLE in the west is about 300 meters higher than the east, and the middle section has an intra-annual variation for about 1500 meters. Considering the RSLE time-series of different subregions, the daily RSLE changes greatly in most months except August. The seasonal differences in snow evolution can be related to what happens in the field that the curve of the snow line in spring is smoother than the curve of the snow line in autumn. It is due to the variability of event-based snowfall in the fall and the gradual depletion of snowfall in the spring. This finding suggests that the reduction in snow duration in these regions can be attributed to earlier spring snowmelt, which is consistent with the studies in other regions by Klein et al. (2016) and Parajka et al. (2010). Multi-year variation can also be determined intuitively with the monthly average RSLE. In the recent autumn, the monthly average RSLE is gradually rising in all the subregions (figure 23), which means a shorter snow cover duration at affected elevations, and decreasing total snow cover area as the previous studies indicated.

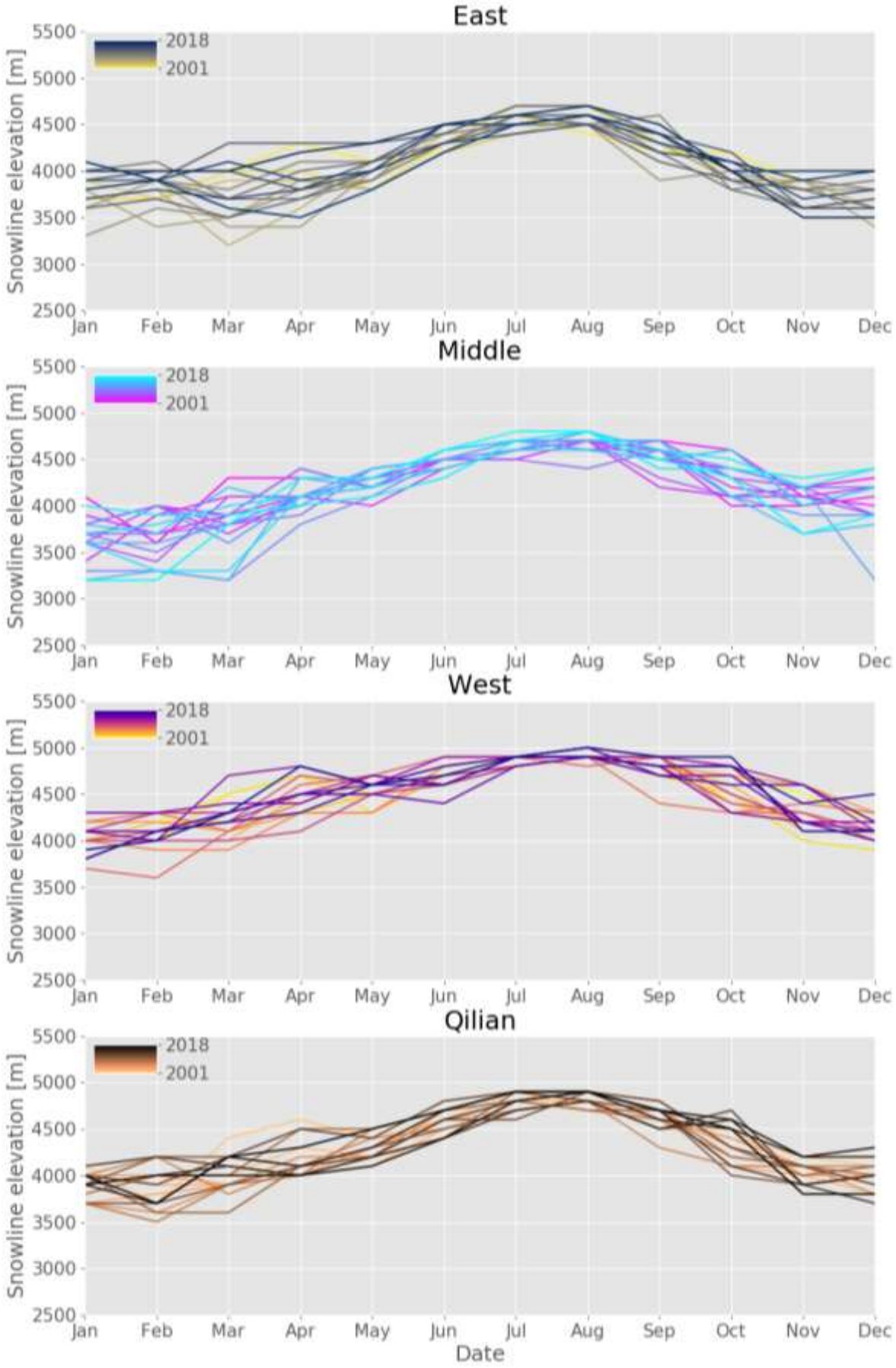

Figure 23. The monthly average RSLE in each subregion and the whole Qilian Mountains region from 2001 to 2018

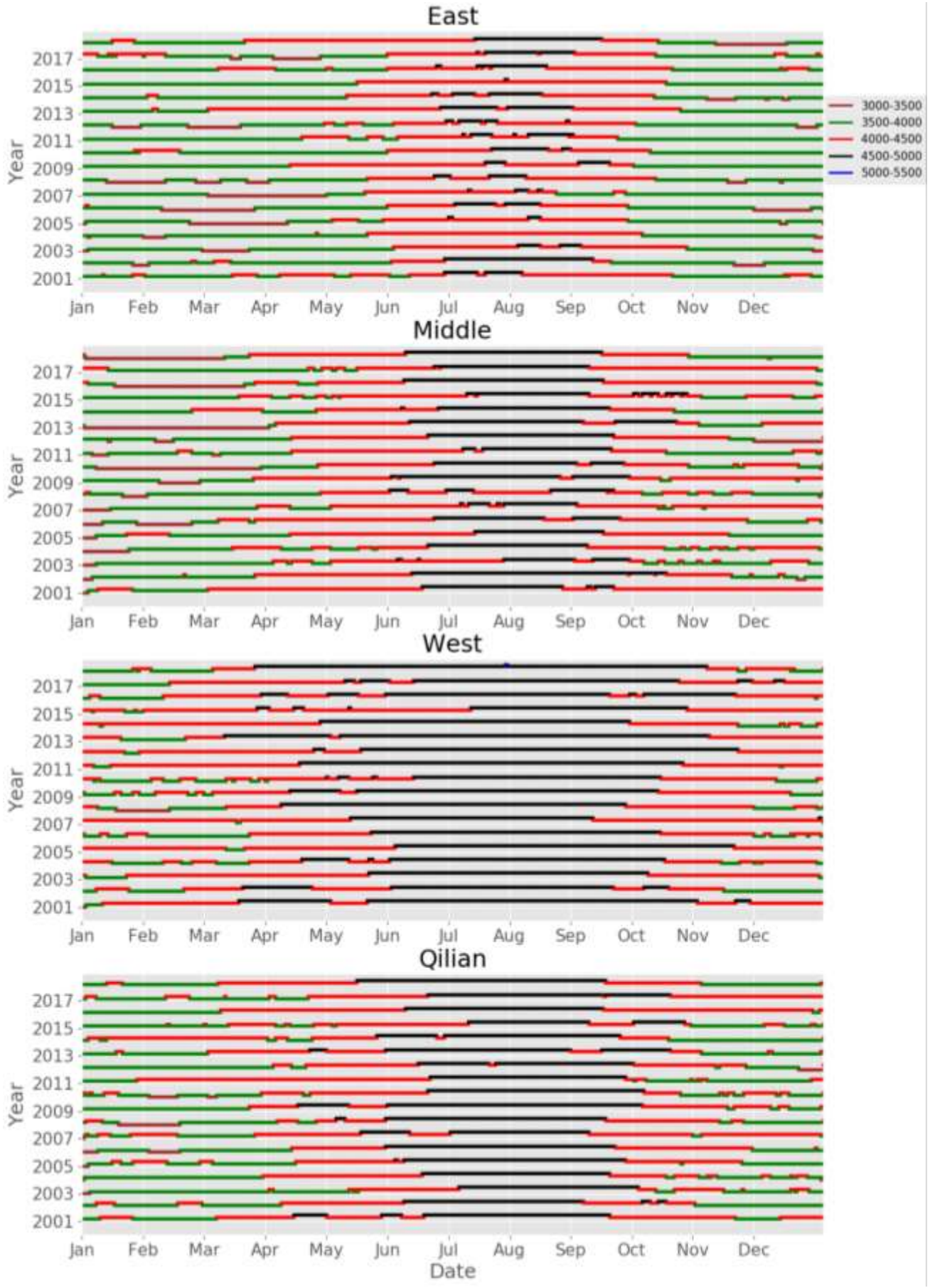

Figure 24. The date when RSLE in the specific elevation range (in m.a.s.l) in each subregion and the whole Qilian Mountains region from 2001 to 2018

Figure 24 shows that the RSLE in each subregion reaches the top in July and August. In the east subregion, the RSLE starts rising in April and dropping in September, while the other subregions start rising earlier in March and dropping later in late September and October. In the west subregion, the drop lasts until the end of November, and the RSLE time-series is more smooth. This regional difference is likely a result of the higher winter precipitation in the east. Overall, at the higher elevation, the snow starting time is earlier, the snow cover ending time is later, and the snow cover duration is longer as we see in figures 14a and 14b.

5.2 Temporal evolution of D_{sc}

The resulting map of average annual D_{sc} in the study period shows similar details compared to the map of snow cover frequency based on MODIS 8-day snow product in previous studies (e.g. Jiang et al., 2016). However, because of the missing station observed data, a quality-check can not be applied, and thus, in the future, we expect to get more ground data for validation of the D_{sc} result in this study.

Summing up all the previous studies on the Qilian Mountains snow cover seasonality available to us, whether they are observational or predictive, disregarding the specific type of metric considered, the condensed message is that annual snow cover is shrinking in the past years and decades on the mountains. This message is supported by our results. In our study, considering the results of the trend analysis maps, we are sure that there is a large regional difference in the change in D_{sc} and the largest change rate (-5 d/year) with a high confidence level (95%) is found in the west of the Qilian Mountains. While some regions have an increasing trend with less than 1 d/year, D_{sc} is declining in most regions, but the confidence level of these increasing/decreasing trends are low. Not only the magnitude of the change but also the level of significance varies greatly across the region, which might be caused by the local topography, vegetation, and small-scale weather environment. The results not only provide spatially reliable information with detail on the rate of change of D_{sc} in the study period but also a good indication of the temporal trend of the snow cover duration in the Qilian Mountains.

Moreover, the declining snow cover in the Qilian Mountains is just an epitome of the Qinghai-Tibet Plateau. Brown and Robinson (2011) emphasized that in the past 90 years,

the snow cover in the northern hemisphere has decreased significantly and has a high level of confidence. In the northern hemisphere, in situ data usually indicate that as the climate warms, the number of snow days and snow depth decreases, especially where the elevation is low or the average temperature is high (Forster et al., 2007). However, the snow on the Tibetan Plateau shows unique characteristics. Qin et al. (2006) suggested increasing snow cover between 1951 and 1997, and western China did not experience a continual decrease in snow cover during the great warming period of the 1980s and 1990s, but Xu et al. (2017) suggested that from 1981 to 2010, in the warm half-year, snow depth and the number of snow cover days showed a significant decreasing trend for most sites. Tang et al. (2013) indicated that about 34.14% area of the QTP presented a declining trend of the number of snow cover days from 2001 to 2011, but only about 5% of them were significant, while Qilian Mountains was one of the regions with the reduction of snow cover.

The previous studies also suggested that the snow cover is expected to shrink further at a higher rate not only in QTP but also in the Qilian Mountains for the next few decades, mainly due to the expectation that the rising of average temperature in the Qilian Mountains will accelerate (Han et al., 2011). We hope that this study will prove useful and spatially clear patterns of this shrinking, along with point information on station observed climate data (e.g. temperature and precipitation forecasts) for the future snow cover variation under climate change.

5.3 Relating D_{sc} to temperature and precipitation

Combining the results of the analysis in subregions and the trend map of D_{sc}, T, and P_c, we can say that, in each subregion, the valley is always less snow-cover than the ridge as the valley has higher temperature especially in the warm half-year. Moreover, the D_{sc} decline of 5 d/year in the west is mainly due to the 0.1-0.2 ℃/year increase in the same location. The results of sensitivities analysis also show that the effects of temperature are more dominant than the effects of precipitation in all subregions. The sensitivities of the P_c show that the sensitivity in the east subregion is much lower than the middle and west, but the extremely low P_c in the west makes the high sensitivity meaningless. Though the precipitation has relatively weak control over the snow cover duration, we

can not ignore that the east subregion has a higher D_{sc} than the west subregion at the same elevation, and the reason for that spatial difference is likely the higher precipitation in the east of the Qilian Mountains.

For elevations below 3000 m.a.s.l., snow melts within a few days after a snowfall, so D_{sc} in this area is unlikely to be directly related to average precipitation and temperature, but extreme events play important roles. The results of sensitivities indicate that D_{sc} is more sensitive to climate change at 3500-5000 m.a.s.l. When the elevation rises above 3500 but below 4500 m.a.s.l., a more continuous snow cover period is expected throughout the season, compared with the lower elevations. The properties of these periods (i.e. length and number of D_{sc} throughout the year) are controlled and can be explained by time-series of precipitation and temperature. However, the temperature can be higher than 0 °C at some time, and some melting/accumulation processes may occur throughout the season like at lower elevations, but these processes are not easy for the optical telemetry to capture e.g. they may be blocked by the cloud and filled as gaps. When the elevation rises until reaching the glacier (i.e. about 5000 m.a.s.l), the accumulation processes are more likely to be continuous since the temperature throughout the season is always below 0 °C. It leads to a continuous snow cover period, and all solid deposits accumulate and stay in the snowpack until the start of melting in spring. As a result, precipitation does contribute to some share of these D_{sc} changes throughout elevations.

Moreover, some previous studies on the QTP suggested that precipitation plays an important role in the snow cover. Gao et al. (2012) indicated that the length of the snow-cover season appeared to be decreasing at lower elevation because of the increase in air temperatures, while at higher elevations the increase in precipitation appeared to compensate for the increase in air temperature such that the length of the snow-free period had decreased. A study on Tianshan (Guo and Li, 2014) showed that the precipitation contributed more to the snow cover at a higher elevation, while it is still affected by the air temperature. The summer monsoon precipitation was closely associated with the snow cover period over QTP not only in the interannual variation but also in the decadal variation (Chen and Wu, 2000). The interaction between precipitation and temperature can explain the higher D_{sc} at the same elevation in the east subregion since the east subregion has increasing precipitation to offset the effects of temperature, while the west subregion has almost no precipitation in the cold half-year. Therefore, this

study partially finds the correlation between the regional differences in D_{sc} changes and the interaction between temperature and precipitation. According to the trajectory of any variable, the interaction between T and P_c can offset the impact of a warming climate in the east of the Qilian Mountains. Besides, the results indicate that this interaction may cause D_{sc} in some regions to be more sensitive to climate change during the study period. For example, the southern slope of the main mountains in the west subregion has a high standard deviation on D_{sc} for more than 40 days.

Furthermore, the statistical analyses of temperature and precipitation have shown that 0.1-0.2 °C/year temperature rising in the west and 1-2 (mm/year)/year precipitation increasing in the east was stable and significant in the past 18 years, and will be consistent for the several years in the future. Thus, the temporal trend of D_{sc} obtained in this study is still applicable in the climate conditions for future years.

5.4 Relating D_{sc} to hillshade

The hillshade shows itself an important topographic factor of D_{sc} that the area with relatively medium hillshade has the lowest D_{sc}. However, this interesting result is not that confident due to the lack of detail from the ground measurement data, and it needs more validation in future observation.

5.5 Review of the method

Using the RSLE method (Krajci et al., 2014) has significant advantages over snow mapping techniques that only process 2D or "planar" images for several reasons. By merging elevation information or 3D space, this variable is strongly related to the natural process of snow distribution, e.g. rising and descending snow lines due to snow melting and accumulation. Another advantage of applying this method is the implicit reduction of cloud cover. Besides, many metrics describing the snow distribution pattern in space and time, including the elevation of the snow line itself, can be derived directly from the generated RSLE time-series. However, RSLE should only be considered as a natural surrogate value due to factors e.g. preferential accumulation and snow deposition since it is the average snow line in predefined regions.

Moreover, in the RSLE method, a key assumption that is not always realized on the ground, especially during melting: all areas above the snow line are snow-covered, and all areas below are snow-free. In Allchin and Déry's (2017) proposal, these areas should be considered and referred to as "snow-based" and "non-snow-based". The spatial scale and accuracy requirements of this assumption, which is a critical problem, must be carefully considered before applying this method. For example, for the studies on a spatial scale much smaller than the selected level of discretization, the accuracy requirements will not be met (small-scale hydrology, avalanche research, etc.).

In this study, we are missing the station observed snow cover data to do the comparison between the station and D_{sc} time-series. For the comparison, if possible, we must remind that station point is being compared to the average value of a region, which is derived from a 500 m grid for a 100 m elevation zone. Also, we should remind that a time-series of 18 years may not be long enough to find a confident connection to climate change effects if short-term trends happen to be embedded in long-term trends pointing in the opposite direction.

5.6 Further applications

The combination of the RSLE method and MODIS dataset in this study can well describe the spatiotemporal pattern of snow cover duration. This method can be used to draw snow line elevation and snow cover situation at daily time steps across different scales (from single-basin to multi-catchment). For possible further applications, it can be tested and used as a spatially explicit extension of long-term station data to study the impact of climate change on snow distribution. As an agent of a snow-based hydrology model e.g.snow water equivalent (SWE), snow cover situations can be useful for calibration in hydrological models. It can also provide relatively confident and valuable input for SWE modeling and research involving albedo backscattering as an element of the Earth's energy balance, or for snow output verification of other snow-related models and data products.

6 Conclusions

The RSLE method with MODIS snow products is applied in the Qilian Mountains for obtaining the cloud-free snow line in a daily temporal resolution. After that, the number of annual snow cover days is obtained in a 500 m x 500 m spatial resolution. The next step is connecting the result of snow cover duration to the remote-sensing data of temperature and precipitation for a temporal and spatial correlation. Besides, we try to link the hillshade to the snow cover duration. We discover:

a) The RSLE has raised about 100-200 meters in July and August in the past 18 years. The east subregion has its RSLE about 300 meters lower than the west subregion over the year due to the overall lower elevation and higher cold half-year precipitation. Also, the RSLE in the east subregion is steeper than the west because of the 15-30 days later snow melting and the 15-30 days earlier snow accumulation. The middle subregion has very few snow cover in the warm half-year. A clear elevation gradient is found in the snow starting time (earlier at higher elevation), snow cover ending time (later at higher elevation), and snow cover duration (longer at higher elevation).

b) Across the entire Qilian Mountains, D_{sc} is about 20-40 days at elevations below 3500 m.a.s.l, about 130 days at 4500 m.a.s.l, and more than 300 days above 5000 m.a.s.l. In the west, D_{sc} is lower than the east at the same elevation, and the largest difference is about 200 days at 4300 m.a.s.l. The middle subregion has D_{sc} lower than the west below 4000 m.a.s.l, but higher above that elevation. Throughout the Qilian Mountains, on the 3500-4500 m.a.s.l hillside regions in the west section, the number of annual snow cover (D_{sc}) has a considerable negative trend about -5 d/year with a 95% level of confidence, while the other region does not have significant trends of D_{sc}. This considerably decreasing D_{sc} is led by the rising of the local land surface temperature.

c) The temperature T has strong, stable and negative effects on D_{sc} in all the subregions, no matter across the years, while the influence of cold half-year precipitation P_c is positive but quite unstable. Throughout the elevation, D_{sc} is sensitive to climate change at 3500-5000 m.a.s.l. For the Qilian Mountains, the temperature rising is the main reason for the snow cover duration to decrease in the study period. Precipitation can offset some of the effects of temperature rising in the east. However, the precipitation in the west is extremely low, and thus, the negative trends of D_{sc} appear only there.

d) The hillshade can be related to D_{sc} that the lowest D_{sc} happens at not the lightest but the relatively medium hillshade. It can be explained by the correlation between hillshade and elevation, that the highest peaks i.e. glaciers of the mountains are always not blocked by the shadow.

Bibliography

Steiger, Robert. "The impact of snow scarcity on ski tourism: an analysis of the record warm season 2006/2007 in Tyrol (Austria)." *Tourism Review* 66.3 (2011): 4-13.

Dadic, R., et al. "Wind influence on snow depth distribution and accumulation over glaciers." *Journal of Geophysical Research: Earth Surface* 115.F1 (2010).

Rinehart, Alex J., Enrique R. Vivoni, and Paul D. Brooks. "Effects of vegetation, albedo, and solar radiation sheltering on the distribution of snow in the Valles Caldera, New Mexico." *Ecohydrology: Ecosystems, Land and Water Process Interactions, Ecohydrogeomorphology* 1.3 (2008): 253-270.

Jost, Georg, et al. "The influence of forest and topography on snow accumulation and melt at the watershed-scale." *Journal of Hydrology* 347.1-2 (2007): 101-115.

Ellis, C. R., et al. "Simulation of snow accumulation and melt in needleleaf forest environments." *Hydrology and Earth System Sciences* 14.6 (2010): 925-940.

Deems, Jeffrey S., et al. "Combined impacts of current and future dust deposition and regional warming on Colorado River Basin snow dynamics and hydrology." *Hydrology and Earth System Sciences* 17.11 (2013): 4401-4413.

Kunkel, Kenneth E., et al. "Trends and extremes in Northern Hemisphere snow characteristics." *Current Climate Change Reports* 2.2 (2016): 65-73.

Hori, Masahiro, et al. "A 38-year (1978–2015) Northern Hemisphere daily snow cover extent product derived using consistent objective criteria from satellite-borne optical sensors." *Remote sensing of environment* 191 (2017): 402-418.

Brown, Ross D., and David A. Robinson. "Northern Hemisphere spring snow cover variability and change over 1922–2010 including an assessment of uncertainty." *The Cryosphere* 5.1 (2011): 219-229.

Mudryk, L. R., et al. "Snow cover response to temperature in observational and climate model ensembles." *Geophysical Research Letters* 44.2 (2017): 919-926.

Parajka, J., and G. Blöschl. "Validation of MODIS snow cover images over Austria." *Hydrology and Earth System Sciences Discussions* 3.4 (2006): 1569-1601.

Parajka, J., and G. Blöschl. "The value of MODIS snow cover data in validating and calibrating conceptual hydrologic models." *Journal of Hydrology* 358.3-4 (2008): 240-258.

Brown, Ross D., and Philip W. Mote. "The response of Northern Hemisphere snow cover

to a changing climate." *Journal of Climate* 22.8 (2009): 2124-2145.

Allchin, Michael I., and Stephen J. Déry. "A spatiotemporal analysis of trends in Northern Hemisphere snow-dominated area and duration, 1971–2014." *Annals of Glaciology* 58.75pt1 (2017): 21-35.

Andreadis, Konstantinos M., and Dennis P. Lettenmaier. "Assimilating remotely sensed snow observations into a macroscale hydrology model." *Advances in water resources* 29.6 (2006): 872-886.

Barnett, Tim P., Jennifer C. Adam, and Dennis P. Lettenmaier. "Potential impacts of a warming climate on water availability in snow-dominated regions." *Nature* 438.7066 (2005): 303.

Berghuijs, W. R., R. A. Woods, and M. Hrachowitz. "A precipitation shift from snow towards rain leads to a decrease in streamflow." *Nature Climate Change* 4.7 (2014): 583.

Berghuijs, Wouter R., et al. "Patterns of similarity of seasonal water balances: A window into streamflow variability over a range of time scales." *Water Resources Research* 50.7 (2014): 5638-5661.

Crawford, Christopher J. "MODIS Terra Collection 6 fractional snow cover validation in mountainous terrain during spring snowmelt using Landsat TM and ETM+." *Hydrological processes* 29.1 (2015): 128-138.

Déry, Stephen J., and Ross D. Brown. "Recent Northern Hemisphere snow cover extent trends and implications for the snow-albedo feedback." *Geophysical Research Letters* 34.22 (2007).

Dietz, Andreas J., Christoph Wohner, and Claudia Kuenzer. "European snow cover characteristics between 2000 and 2011 derived from improved MODIS daily snow cover products." *Remote Sensing* 4.8 (2012): 2432-2454.

Dong, Chunyu, and Lucas Menzel. "Producing cloud-free MODIS snow cover products with conditional probability interpolation and meteorological data." *Remote Sensing of Environment* 186 (2016): 439-451.

Fernandes, Richard, et al. "Controls on Northern Hemisphere snow albedo feedback quantified using satellite Earth observations." *Geophysical Research Letters* 36.21 (2009).

Fu, Pinde, and Paul M. Rich. "A geometric solar radiation model with applications in agriculture and forestry." *Computers and electronics in agriculture* 37.1-3 (2002): 25-35.

Gafurov, Abror, and András Bárdossy. "Cloud removal methodology from MODIS snow cover product." *Hydrology and Earth System Sciences* 13.7 (2009): 1361-1373.

Gao, Hongkai, et al. "Climate controls how ecosystems size the root zone storage capacity at catchment scale." *Geophysical Research Letters* 41.22 (2014): 7916-7923.

Hall, Dorothy K., and George A. Riggs. "Accuracy assessment of the MODIS snow products." *Hydrological Processes: An International Journal* 21.12 (2007): 1534-1547.

Hall, Dorothy K., et al. "MODIS snow cover products." *Remote sensing of Environment* 83.1-2 (2002): 181-194.

Härer, Stefan, et al. "On the need for a time-and location-dependent estimation of the NDSI threshold value for reducing existing uncertainties in snow cover maps at different scales." *The Cryosphere* 12.5 (2018): 1629-1642.

Hrachowitz, M., et al. "A decade of Predictions in Ungauged Basins (PUB)—a review." *Hydrological sciences journal* 58.6 (2013): 1198-1255.

Immerzeel, Walter W., et al. "Large-scale monitoring of snow cover and runoff simulation in Himalayan river basins using remote sensing." *Remote sensing of Environment* 113.1 (2009): 40-49.

Laaha, Gregor, et al. "A three-pillar approach to assessing climate impacts on low flows." *Hydrology and Earth System Sciences* 20.9 (2016): 3967-3985.

Painter, Thomas H., et al. "Retrieval of subpixel snow cover area, grain size, and albedo from MODIS." *Remote Sensing of Environment* 113.4 (2009): 868-879.

Parajka, J., et al. "MODIS snow cover mapping accuracy in a small mountain catchment–comparison between open and forest sites." *Hydrology and Earth System Sciences* 16.7 (2012): 2365-2377.

Räisänen, Jouni. "Warmer climate: less or more snow?." *Climate Dynamics* 30.2-3 (2008): 307-319.

Rittger, Karl, Thomas H. Painter, and Jeff Dozier. "Assessment of methods for mapping snow cover from MODIS." *Advances in Water Resources* 51 (2013): 367-380.

Tang, Zhiguang, et al. "Spatiotemporal changes of snow cover over the Tibetan plateau based on cloud-removed moderate resolution imaging spectroradiometer fractional snow cover product from 2001 to 2011." *Journal of Applied Remote Sensing* 7.1 (2013): 073582.

Theil, Henri. "Economic forecasts and policy." (1961).

Tomaszewska, Monika A., and Geoffrey M. Henebry. "Changing snow seasonality in the highlands of Kyrgyzstan." *Environmental Research Letters* 13.6 (2018): 065006.

Lehning, M., et al. "Inhomogeneous precipitation distribution and snow transport in steep terrain." *Water Resources Research* 44.7 (2008).

Madani, Kaveh, and Jay R. Lund. "Estimated impacts of climate warming on California's high-elevation hydropower." *Climatic Change* 102.3-4 (2010): 521-538.

Mankin, Justin S., et al. "The potential for snow to supply human water demand in the present and future." *Environmental Research Letters* 10.11 (2015): 114016.

Molini, Annalisa, Gabriel G. Katul, and Amilcare Porporato. "Maximum discharge from snowmelt in a changing climate." *Geophysical Research Letters* 38.5 (2011).

Mudryk, L. R., et al. "Characterization of Northern Hemisphere snow water equivalent datasets, 1981–2010." *Journal of Climate* 28.20 (2015): 8037-8051.

Parajka, J., and G. Blöschl. "Spatio-temporal combination of MODIS images–potential for snow cover mapping." *Water resources research* 44.3 (2008).

Chang, Ni-Bin, and Yang Hong. Multiscale hydrologic remote sensing: Perspectives and applications. CRC Press, 2012.

Sospedra-Alfonso, Reinel, Joe R. Melton, and William J. Merryfield. "Effects of temperature and precipitation on snowpack variability in the Central Rocky Mountains as a function of elevation." *Geophysical Research Letters* 42.11 (2015): 4429-4438.

Stehr, Alejandra, and Mauricio Aguayo. "Snow cover dynamics in Andean watersheds of Chile (32.0–39.5 S) during the years 2000–2016." *Hydrology and Earth System Sciences* 21.10 (2017): 5111-5126.

Huning, Laurie, and A. AghaKouchak. "Spatial and Temporal Variability of Snow Drought Characteristics." *AGU Fall Meeting Abstracts*. 2018.

Huning, Laurie, Amir AghaKouchak, and Steven A. Margulis. "Progress in Remote Sensing-Based Snow Hydrology and Its Applications." *AGU Fall Meeting Abstracts*. 2018.

Held, Isaac M., and Brian J. Soden. 'Robust responses of the hydrological cycle to global warming.' *Journal of climate* 19.21 (2006): 5686-5699.

Zhai, Panmao, et al. 'Trends in total precipitation and frequency of daily precipitation extremes over China.' *Journal of climate* 18.7 (2005): 1096-1108.

Shi, Yafeng, et al. 'Recent and future climate change in northwest China.' *Climatic*

change 80.3-4 (2007): 379-393.

Li, Xiao-Yan, et al. 'Lake-level change and water balance analysis at Lake Qinghai, west China during recent decades.' *Water Resources Management* 21.9 (2007): 1505-1516.

Luo, C., et al. 'Monitoring of water surface area in Lake Qinghai from 1974 to 2016.' *Journal of Lake Science* 29.5 (2017): 1245-1253.

Zhang, Guoqing, et al. 'Water level variation of Lake Qinghai from satellite and in situ measurements under climate change.' *Journal of Applied Remote Sensing* 5.1 (2011): 053532.

China Institute of Water Resources and Hydropower Research (2012). *Qinghai Province Water Conservancy Development Strategic Plan.* Retrieved from: http://www.iwhr.com/zgskyww/rootfiles/2012/08/03/1342498798969043-1342498798971730.pdf.

Qunzhi, Zeng, et al. 'Satellite snow cover monitoring in the Qilian Mountains and an analysis for characteristics of stream snow-melt run-off in the Hexi region, Gansu, China.' *Annals of glaciology* 9 (1987): 225-228.

Qian, Chen, and Chen Tianyu. 'Climatological analysis of seasonal snow resources in the Qilian Mountains.' *The J Chinese Geography* 2.1 (1991): 59-77.

Zhigang, Wei, et al. 'Spatial distributions and interdecadal variations of the snow at the Tibetan Plateau weather stations.' *Chinese Journal of Atmospheric Sciences-Chinese Edition* 26.4 (2002): 496-508.

Guo, N., L. F. Yang, and M. X. Li. 'Study of changes of vegetation and snow area in the Qilian Mountains using meteorology satellite data.' *J Appl Meteorol Sci* 14.6 (2003): 700-707.

Squires, Victor, et al., eds. *Towards sustainable use of rangelands in North-West China*. Springer Science & Business Media, 2010.

Hall, D. K., V. V. Salomonson, and G. A. Riggs. 2016. *MODIS/Terra Snow cover Daily L3 Global 500 m Grid. Version 6*. Boulder, Colorado USA: NASA National Snow and Ice Data Center Distributed Active Archive Center.

Global Multi-resolution Terrain Elevation Data 2010 courtesy of the U.S. Geological Survey

Sun Meiping, et al. 'Study on maximum precipitation height zone in the Qilian Mountains area based on TRMM precipitation data. ' *Journal of Natural Resources*, 2019,34(3): 646-

657

Ke, L. H., et al. ‘Reconstruction of MODIS land surface temperature in Northeast Qinghai-Xizang Plateau and its comparison with air temperature.’ *Plateau Meteorology* 30.2 (2011): 277-287.

Yu, Wenping, et al. ‘Validation of MODIS land surface temperature products using ground measurements in the Heihe River Basin, China.’ *Remote Sensing for Agriculture, Ecosystems, and Hydrology XIII*. Vol. 8174. International Society for Optics and Photonics, 2011.

Gorelick, N., Hancher, M., Dixon, M., Ilyushchenko, S., Thau, D., & Moore, R. (2017). Google Earth Engine: Planetary-scale geospatial analysis for everyone. *Remote Sensing of Environment*.

Hao, X. H., Jian Wang, and H. Y. Li. ‘Evaluation of the NDSI threshold value in mapping snow cover of MODIS—A case study of snow in the Middle the Qilian Mountains.’ *J. Glaciol. Geocryol* 30.1 (2008): 132-138.

Parajka, J., et al. ‘A regional snow-line method for estimating snow cover from MODIS during cloud cover.’ *Journal of Hydrology* 381.3-4 (2010): 203-212.

Krajčí, Pavel, et al. ‘Estimation of regional snowline elevation (RSLE) from MODIS images for seasonally snow cover mountain basins.’ *Journal of Hydrology* 519 (2014): 1769-1778.

Krajčí, Pavel, Ladislav Holko, and Juraj Parajka. ‘Variability of snow line elevation, snow cover area and depletion in the main Slovak basins in winters 2001–2014.’ *Journal of hydrology and hydromechanics* 64.1 (2016): 12-22.

Zhang, Jie, Tao Han, and Jian Wang. ‘Changes of snow cover area and snowline elevation in the Qilian Mountains, 1997-2004.’ *Journal of Glaciology and Geocryology* 27.5 (2005): 650-654.

Cai, D. H., et al. ‘The spatial and temporal variations of snow cover over the Qilian Mountains based on MODIS data.’ *Journal of Glaciology and Geocryology* 31.6 (2009): 1028-1036.

Wang, X., et al. ‘Remote Sensing Research of Snow cover Distribution and Variation in the Qilian Mountains in the Winter Half Year of 1996-2002.’ *Plateau Meteorology* 29.2 (2010): 366-372.

Han, LanYing, et al. ‘The snow coverage change in eastern section of Qilian Mountain

and its response to regional climate.' *Journal of Arid Land Resources and Environment* 25.5 (2011): 109-112.

Jiang, Youyan, et al. 'Variation in the snow cover on the Qilian Mountains and its causes in the early 21st century.' *Geomatics, Natural Hazards and Risk* 7.6 (2016): 1824-1834.

You, L.; Yang, J. *Geomorphology in China*; Science Press: Beijing, China, 2013.

Shi, Yafeng, Chaohai Liu, and Ersi Kang. 'The glacier inventory of China.' *Annals of Glaciology* 50.53 (2009): 1-4.

Tian, Hongzhen, Taibao Yang, and Qinping Liu. 'Climate change and glacier area shrinkage in the Qilian Mountains, China, from 1956 to 2010.' *Annals of Glaciology* 55.66 (2014): 187-197.

Sun, Meiping, et al. 'Glacier changes in the Qilian Mountains in the past half-century: Based on the revised First and Second Chinese Glacier Inventory.' *Journal of Geographical Sciences* 28.2 (2018): 206-220.

Brown, Ross D., and David A. Robinson. 'Northern Hemisphere spring snow cover variability and change over 1922–2010 including an assessment of uncertainty.' *The Cryosphere* 5.1 (2011): 219-229.

Forster, Piers, et al. 'Changes in atmospheric constituents and in radiative forcing. Chapter 2.' *Climate Change 2007. The Physical Science Basis*. 2007.

Dahe, Qin, Liu Shiyin, and Li Peiji. 'Snow cover distribution, variability, and response to climate change in western China.' *Journal of climate* 19.9 (2006): 1820-1833.

Xu, Wenfang, et al. 'Spatial-temporal variability of snow cover and depth in the Qinghai–Tibetan Plateau.' *Journal of Climate* 30.4 (2017): 1521-1533.

Tang, Zhiguang, et al. 'Spatiotemporal changes of snow cover over the Tibetan plateau based on cloud-removed moderate resolution imaging spectroradiometer fractional snow cover product from 2001 to 2011.' *Journal of Applied Remote Sensing* 7.1 (2013): 073582.

Gao, Jie, et al. 'Spatiotemporal distribution of snow in eastern Tibet and the response to climate change.' *Remote Sensing of Environment* 121 (2012): 1-9.

Guo, Lingpeng, and Lanhai Li. 'Variation of the proportion of precipitation occurring as snow in the Tian Shan Mountains, China.' *International Journal of Climatology* 35.7 (2015): 1379-1393.

Wu, Zhiwei, et al. 'Possible association of the western Tibetan Plateau snow cover with

the decadal to interdecadal variations of northern China heatwave frequency.' *Climate dynamics* 39.9-10 (2012): 2393-2402.

Chen, Lieting, and Renguang Wu. 'Interannual and decadal variations of snow cover over Qinghai-Xizang Plateau and their relationships to summer monsoon rainfall in China.' *Advances in Atmospheric Sciences volume.* 17(2000): 18-30.

A Sensitivities of annual accumulated precipitation

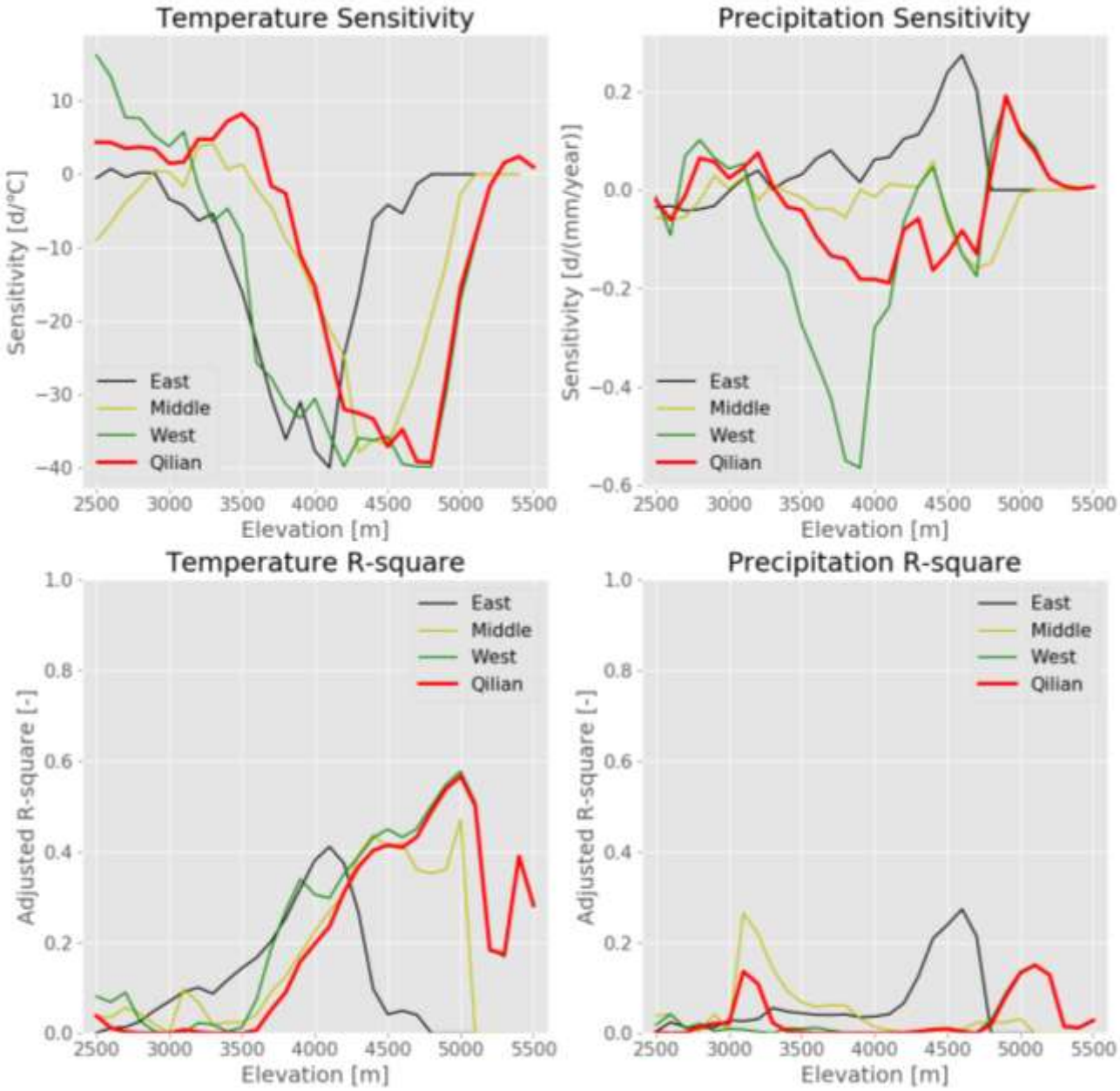

Figure A-1. The sensitivity and R-square of the D_{sc} to temperature and annual accumulated precipitation through different elevations in each subregion and the Qilian Mountains region

In figure A-1, comparing to the results in section 4.3.3 (figure 19), the sensitivities and R-square of the temperature does not change much. However, throughout the elevations, the sensitivities of the middle, west and the whole Qilian Mountains have dropped below zero. That means the negative effects of the precipitation on snow cover duration and is caused by the high consistency between the temperature and annual accumulated precipitation. Moreover, the R-square of annual accumulated precipitation is much lower, especially in the middle and west subregions, which means the effects of cold half-year

precipitation are concealed by the warm half-year precipitation, and the effects of precipitation become ignorable throughout the elevations.

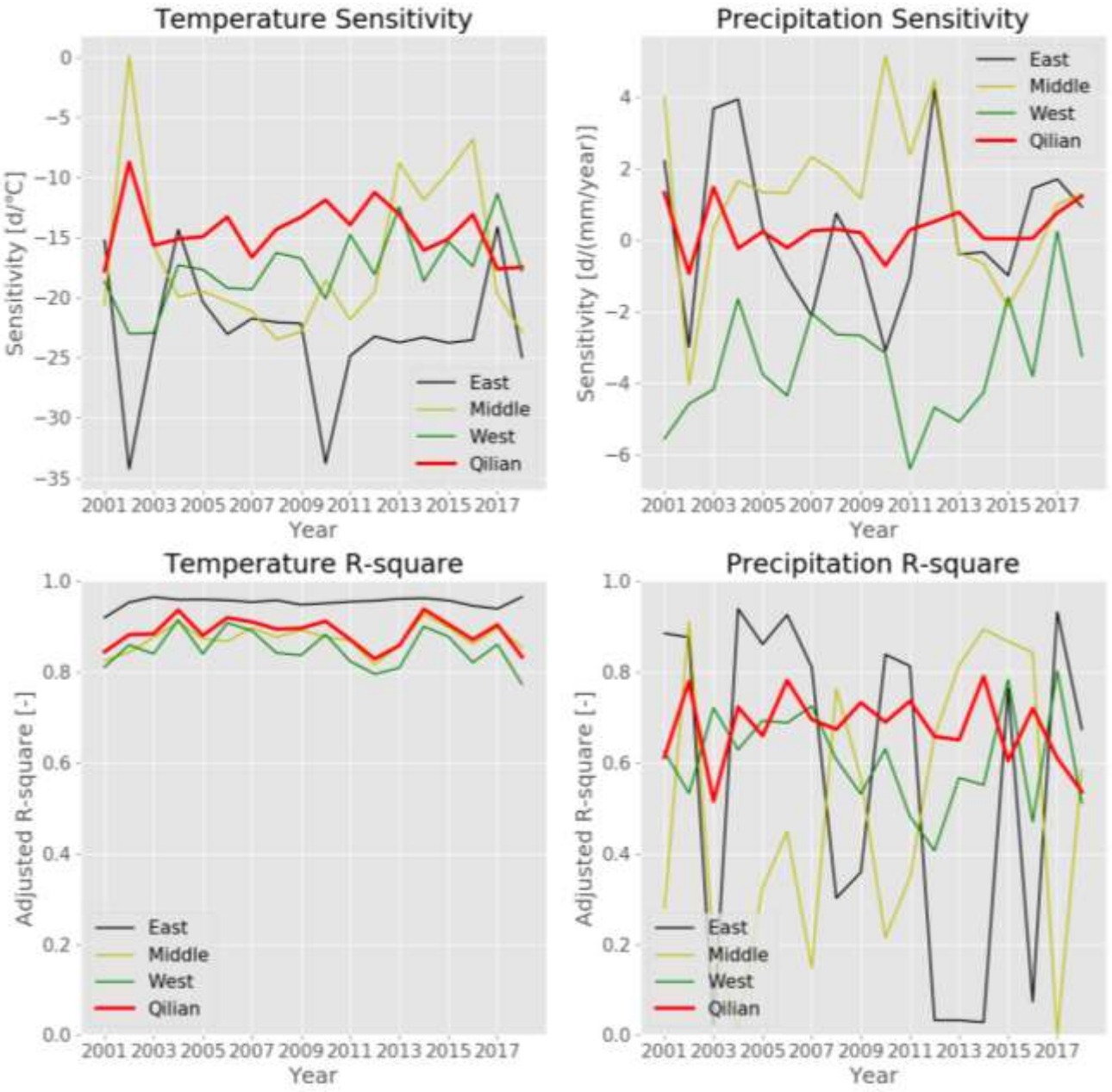

Figure A-2. The sensitivity and R-square of the D_{sc} to temperature and annual accumulated precipitation through different years in each subregion and the Qilian Mountains region

Figure A-2 shows similar results about temperature comparing to figure 20, but much lower sensitivities of annual accumulated precipitation. Even though the R-square in the whole Qilian Mountains becomes more stable (about 0.7), the extremely low sensitivities (less than 1 in absolute value) make the annual accumulated precipitation unimportant to the temporal variation of D_{sc}. Overall, the annual accumulated precipitation should be replaced by the cold half-year precipitation in our analysis.

B Seasonality of D_{sc} and hillshade

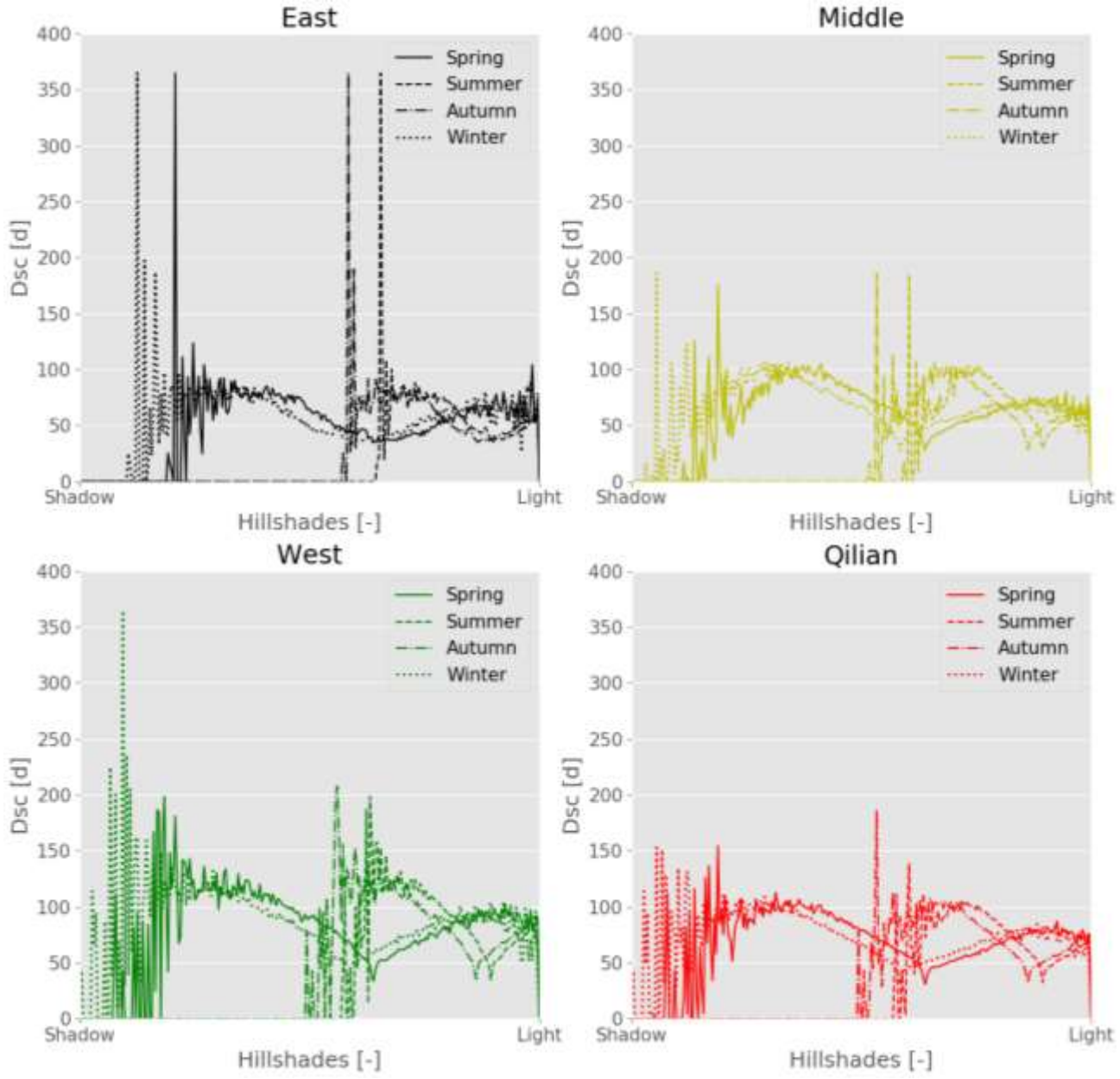

Figure B-1. In each subregion and the entire Qilian Mountains, the correlation between hillshade and the average number of annual snow cover days in 2001-2018 period

Figure B-1 and B-2 gives the same result as we mentioned in section 4.4 that, in all regions, the area of D_{sc} moves from shadow to light in the snow melting period (spring to summer), and moves from light to shadow in the snow accumulation period (autumn to winter). Thus, the D_{sc}-hillshade curves have shown the same seasonal variation as their area variation.

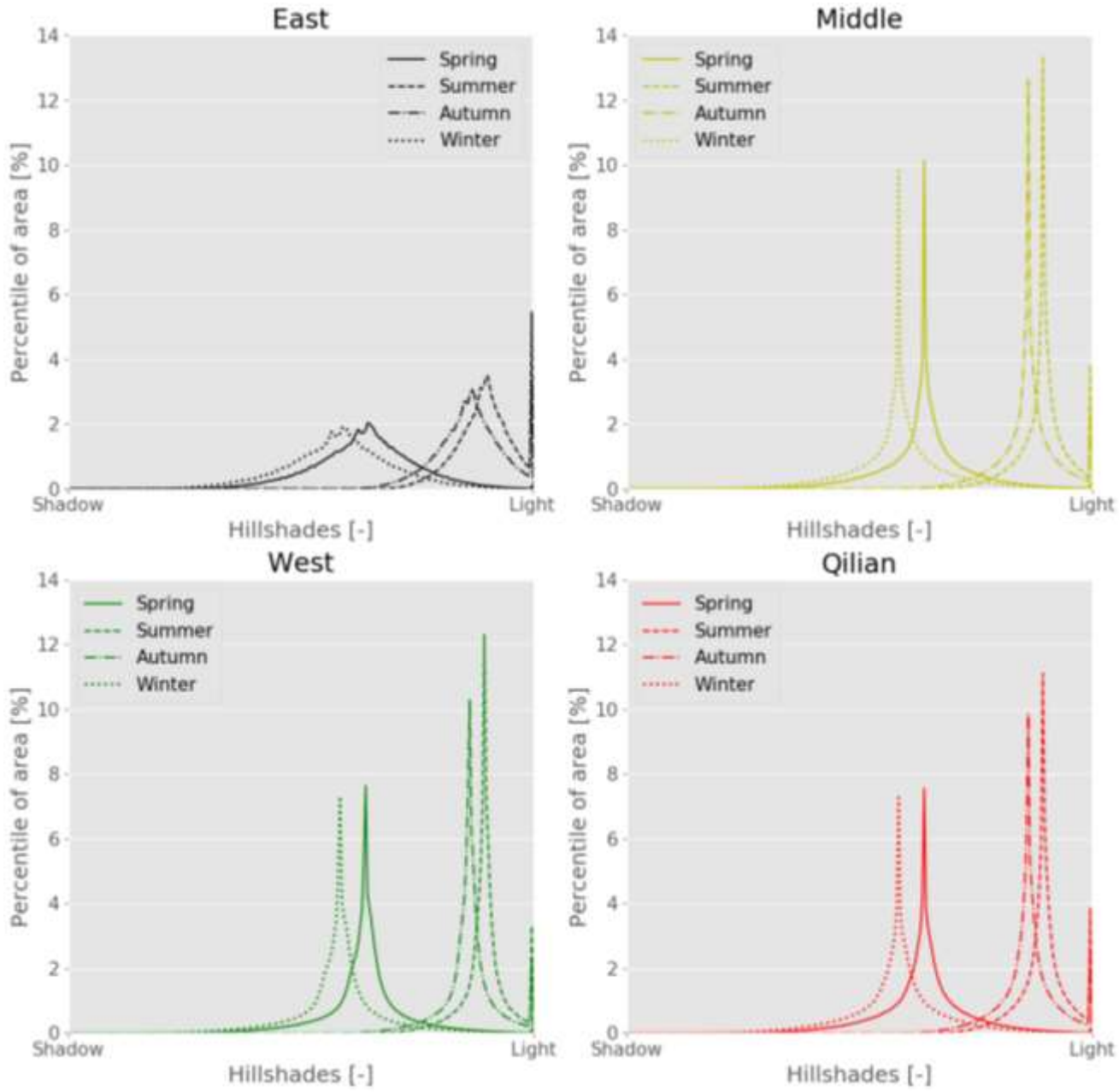

Figure B-2. In each subregion and the entire Qilian Mountains, the average percentiles of the area of different hillshade in 2001-2018 period